

ACCEPTED MANUSCRIPT • OPEN ACCESS

## Heatwave Intensification and Regional Vulnerability Across Texas Under Recent Climate Warming

To cite this article before publication: Deen Dayal *et al* 2026 *Environ. Res. Commun.* in press <https://doi.org/10.1088/2515-7620/ae6a64>

### Manuscript version: Accepted Manuscript

Accepted Manuscript is “the version of the article accepted for publication including all changes made as a result of the peer review process, and which may also include the addition to the article by IOP Publishing of a header, an article ID, a cover sheet and/or an ‘Accepted Manuscript’ watermark, but excluding any other editing, typesetting or other changes made by IOP Publishing and/or its licensors”

This Accepted Manuscript is © 2026 The Author(s). Published by IOP Publishing Ltd.



As the Version of Record of this article is going to be / has been published on a gold open access basis under a CC BY 4.0 licence, this Accepted Manuscript is available for reuse under a CC BY 4.0 licence immediately.

Everyone is permitted to use all or part of the original content in this article, provided that they adhere to all the terms of the licence <https://creativecommons.org/licenses/by/4.0>

Although reasonable endeavours have been taken to obtain all necessary permissions from third parties to include their copyrighted content within this article, their full citation and copyright line may not be present in this Accepted Manuscript version. Before using any content from this article, please refer to the Version of Record on IOPscience once published for full citation and copyright details, as permissions may be required. All third party content is fully copyright protected and is not published on a gold open access basis under a CC BY licence, unless that is specifically stated in the figure caption in the Version of Record.

View the [article online](#) for updates and enhancements.

# Heatwave Intensification and Regional Vulnerability Across Texas Under Recent Climate Warming

Deen Dayal<sup>1\*</sup>, Santosh S. Palmate<sup>1,2</sup>, Rosario Sanchez<sup>3</sup>

<sup>1</sup>Texas A&M AgriLife Research, Texas A&M University System, El Paso, Texas 79927, USA

<sup>2</sup>Department of Biological and Agricultural Engineering, Texas A&M University, College Station, Texas 77843, USA

<sup>3</sup>Texas Water Resources Institute, Texas A&M University, College Station, Texas, 77843, USA

\*Corresponding author: deen.dayal@ag.tamu.edu

## Abstract

Heatwaves represent one of the most consequential climate hazards, with profound implications for human health, agriculture, energy demands, and water resources. This study examines the spatiotemporal evolution of heatwaves across Texas from 1980 to 2023 using high-resolution Daymet climate data and a comprehensive suite of indicators derived from the Excess Heat Factor. Heatwave characteristics were assessed in terms of frequency, duration, intensity, and timing of onset, and subsequently integrated to construct a new Composite Heatwave Hazard Indicator (CHI) and heatwave vulnerability index. Results reveal a statistically significant intensification of heatwave activity, with increasing frequency, duration, and magnitude observed across 247, 31, and 184 Texas counties, respectively. The mean annual number of heatwave events rose from 3.6 in the 1980s to 8.9 in the 2020s, while total heatwave days increased from 16.6 to 63.6. The onset of the first annual heatwave advanced by approximately 27 days, shifting from the 109th day of the year in the 1980s to the 81st day in the 2020s, thereby extending seasonal exposure. The duration of the longest annual heatwave also increased substantially, from an average of 6.3 days to 16.3 days. Pronounced regional heterogeneity is evident as west Texas experienced the strongest intensification, central Texas emerged as a hotspot of concurrent increases in frequency and duration, and coastal regions exhibited elevated heatwave characteristics, likely exacerbated by high humidity. The CHI identifies three major high-risk clusters, the Houston metropolitan area, west Texas, and the lower Rio Grande Valley, with peak vulnerability in Harris, and Galveston counties; El Paso and Midland counties; and Hidalgo, and Webb counties, respectively. Collectively, these findings demonstrate the escalating severity and spatial complexity of heatwave hazards in Texas and underscore the urgent need for region-specific adaptation and risk-mitigation strategies under a warming climate.

**Keywords:** Excess Heat Factor; Daymet data; Heatwave hazard; Heatwave vulnerability; Texas.

## 1 Introduction

Heatwaves are among the most severe and high-impact weather extremes, with wide-ranging consequences for humans and natural systems (McGregor, 2024). Generally defined as prolonged periods of anomalously high temperature relative to local climatology, heatwaves can cause sharp increases in morbidity and mortality (Robine et al., 2008; Gasparrini et al., 2015), reduce crop yields and livestock productivity (Lobell et al., 2011; Zampieri et al., 2017), disrupt ecosystems (Allen et al., 2010; Teskey et al., 2015), and strain water and energy resources (Perkins, 2015; Mora et al., 2017). The 2003 European heatwave, the 2010 Russian heatwave, and the 2021 Pacific Northwest heatwave exemplify the devastating societal and economic impacts of such events, resulting in tens of thousands of excess deaths and billions of dollars in damages (Barriopedro et al., 2011; Russo et al., 2015; Philip et al., 2022). Beyond acute consequences, repeated exposure to extreme heat has long-term implications for resilience, water security, and regional climate feedbacks.

Observational evidence shows that heatwaves have increased in frequency, duration, and intensity since the mid-20th century, with climate change acting as the primary driver (IPCC, 2021). Hot extremes are projected to intensify further under continued warming, with the magnitude of change depending on the future emission pathways (Perkins-Kirkpatrick & Lewis, 2020). Increases in the frequency and severity of heatwaves are of particular concern since they scale approximately linearly with global mean temperature rise, leaving little doubt about their inevitability under warming scenarios (Seneviratne et al., 2021). Regional heterogeneity, however, highlights the influence of circulation patterns, land-atmosphere feedbacks, and baseline climate conditions on heatwave characteristics (Fischer et al., 2007; Miralles et al., 2019).

In the continental United States, the southern and central regions, including Texas, are recognized as heatwave hotspots (Angélil et al., 2017; Vose et al., 2017). Texas is the largest state in the continental U.S., with a climatically distinct regions spanning humid coastal areas, subtropical plains, and semi-arid to arid western landscapes. The state's agricultural economy, rapid population growth, and energy-intensive infrastructure make it especially vulnerable to extreme heat. Historical events illustrate these risks as the 2011 Texas heatwave was among the most severe in U.S. history, with record-breaking temperatures, crop and livestock losses of billions of U.S. dollars, and unprecedented stress on water and power systems (Combs, 2012; Nielsen-Gammon, 2012). More recently, prolonged extreme heat has pushed electricity demand to record levels and contributed to excess mortality (EPA, 2022). These episodes underscore the urgency of understanding long-term heatwave dynamics in Texas for climate adaptation and public safety.

Despite recognition of these risks, methodological inconsistencies remain in how heatwaves are defined and quantified. Conventional approaches often rely on exceedance of daily maximum or minimum temperature from fixed thresholds or percentiles of their long-term climatological distribution. However, such approaches fail to capture two critical aspects, short-term acclimatization and the persistence of heat, which are strongly linked to human health impacts

(Perkins and Alexander, 2013). To address these shortcomings, the Excess Heat Factor (EHF) index was developed by Nairn and Fawcett (2013). EHF incorporates two complementary anomalies: (i) the short-term exceedance relative to long-term climatological thresholds, and (ii) the acclimatization anomaly, comparing current conditions with the preceding month. By combining these components, EHF identifies periods of heat stress that are both statistically rare and physiologically burdensome. Applications in Australia, Europe, and Asia have demonstrated its robustness and strong association with heat-related morbidity and mortality (Zhang et al., 2017; Mitchell et al., 2016; Oliveira et al., 2022). However, its application in Texas remains limited (Smith et al., 2013; Habeeb et al., 2015). Several U.S. studies have documented rising trends in extreme heat using station observations and gridded climate products (Peterson et al., 2012; Rupp et al., 2015; Vose et al., 2017). Yet, many analyses operate at relatively coarse spatial scales or emphasize broad indices such as the annual maximum temperature. While valuable for national-scale assessments, these approaches can obscure localized dynamics in heatwave frequency, timing, and duration, factors that are critical in a climatically and socioeconomically diverse state such as Texas. Despite substantial progress in heatwave research, relatively few studies have employed the EHF framework to generate a comprehensive set of standardized heatwave indicators (including frequency, intensity, duration, and timing), which are essential for linking climate extremes to sectoral impacts. Moreover, previous studies have focused on only a single dimension of heatwaves when assessing heatwave hazard, and comprehensive evaluations that integrate multiple aspects of heat stress are largely missing. Additionally, heatwave hazard provides only a partial view, because risk also depends on population exposure and the ability of communities to adapt. This creates a clear need for vulnerability assessments that integrate the multiple dimensions of heatwaves with socioeconomic factors.

To address these gaps, this study provides a high-resolution, multi-dimensional assessment of heatwave hazard and vulnerability across Texas for the period 1980–2023. Specifically, our objectives are to: (i) detect heatwave events using daily gridded temperature from the high-resolution Daymet dataset, and derive a suite of EHF-based indicators capturing heatwave frequency, duration, intensity, and onset timing, (ii) analyze spatial and temporal trends in these indicators using non-parametric statistical methods, (iii) develop a Composite Heatwave Hazard Indicator (CHI) that summarizes multi-dimensional heat stress, and (iv) construct a Heatwave Vulnerability Index (HVI) by integrating CHI with demographic and economic indicators of exposure and adaptive capacity. By combining physiologically relevant heatwave metrics, and a vulnerability assessment framework, this study advances understanding of heatwave risks in Texas and supports the development of targeted adaptation strategies for agriculture, energy systems, public health, and integrated water management.

## 2 Study Area

This study focuses on the state of Texas, United States, which is administratively divided into 254 counties (Figure 1). The state area lies between 106.65°W to 93.50°W longitude and 25.83°N to 36.50°N latitude. Texas spans an area of approximately 695,000 km<sup>2</sup> and exhibits substantial

1  
2  
3 climatic and physiographic diversity. The western part of the state is dominated by arid and semi-  
4 arid desert conditions, while central Texas experiences temperate grasslands and the eastern region  
5 is characterized by a humid subtropical climate. Climatic conditions across Texas show  
6 pronounced gradients in both precipitation and temperature. Annual precipitation exhibits a strong  
7 west–east contrast, with values below 300 mm in the arid Trans-Pecos region and exceeding 1600  
8 mm along the humid Gulf Coast. Mean maximum temperature patterns highlight the north–south  
9 gradient, where cooler conditions ( $<20\text{ }^{\circ}\text{C}$ ) dominate the northern Panhandle and warmer values  
10 ( $>30\text{ }^{\circ}\text{C}$ ) prevail in southern and southwestern Texas. Similarly, mean minimum temperatures  
11 increase from northwest to southeast, ranging from below  $6\text{ }^{\circ}\text{C}$  in the northwestern high plains to  
12 above  $18\text{ }^{\circ}\text{C}$  in the lower Rio Grande Valley. These spatial variations in temperature and  
13 precipitation directly influence the frequency and intensity of heat extremes across the state. Such  
14 heterogeneity in climate makes Texas an ideal case to investigate spatio-temporal dynamics of  
15 extreme events. Given the state’s high exposure to extreme heat and heterogeneity in climate  
16 conditions, a detailed spatiotemporal assessment is essential to understand the patterns and shifts  
17 in climate. Moreover, the county-level analysis provides localized characterization to support  
18 regionally relevant adaptation planning.  
19  
20  
21  
22  
23  
24  
25  
26  
27  
28  
29  
30  
31  
32  
33  
34  
35  
36  
37  
38  
39  
40  
41  
42  
43  
44  
45  
46  
47  
48  
49  
50  
51  
52  
53  
54  
55  
56  
57  
58  
59  
60

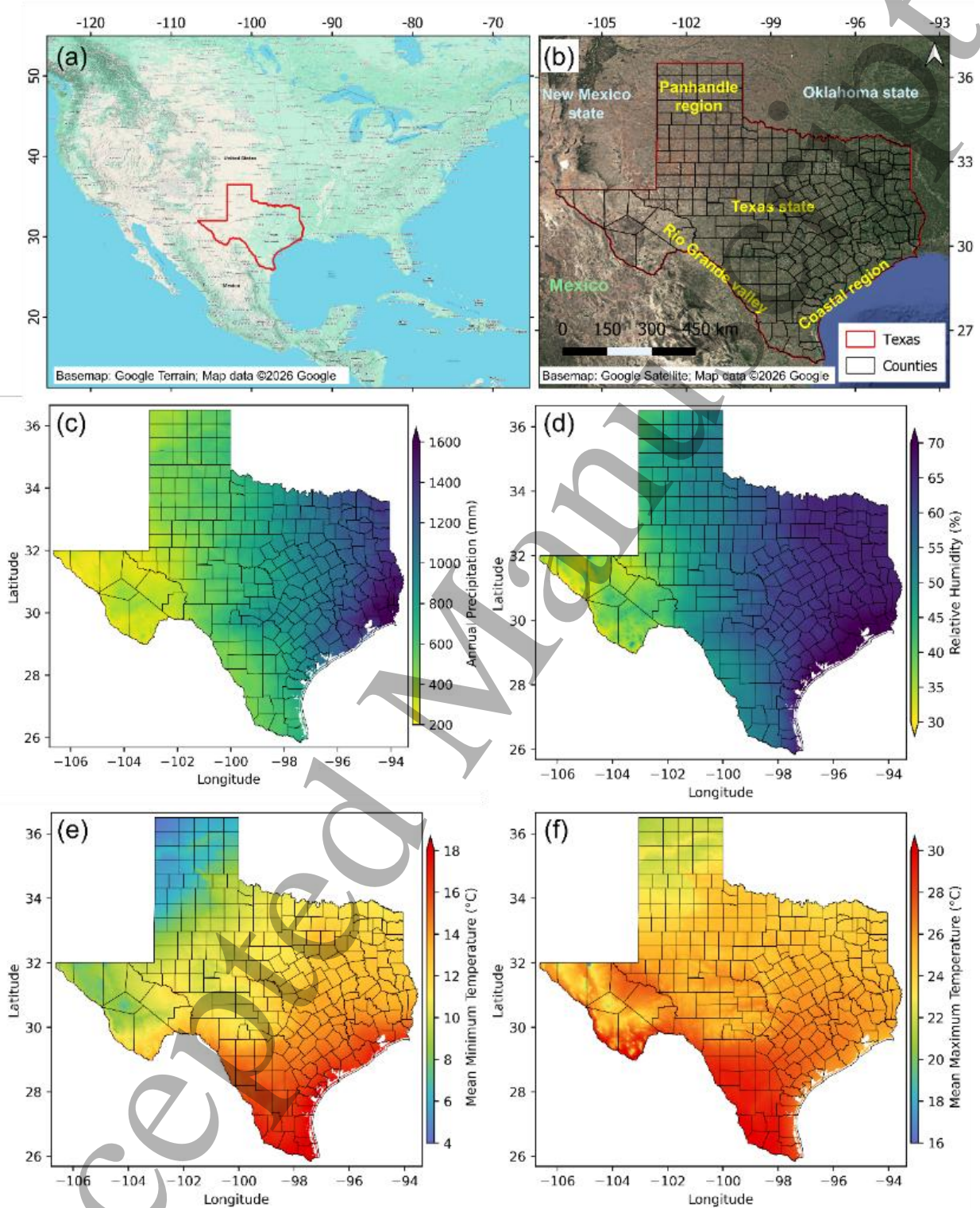


Figure 1: Location of the study area (Texas counties) with annual precipitation, relative humidity, mean maximum temperature, and mean minimum temperature conditions during 1980-2023

### 3 Data and Methods

#### 3.1 Air Temperature, Relative Humidity, Demographic and Economic Data

Daily gridded climate data were sourced from the Daymet Version 4 dataset (Thornton et al., 2022), which provides long-term, high-resolution (1 km × 1 km) meteorological observations for North America from 1980 to the present. Daymet is generated by interpolating ground-based meteorological station observations (obtained from GHCN -Daily and other sources) using a truncated Gaussian weighting filter and elevation corrections from a high-resolution digital elevation model. The dataset includes key meteorological variables such as maximum temperature (Tmax), minimum temperature (Tmin), precipitation, snow water equivalent (swe), shortwave radiation (srad), water vapor pressure (vp), and day length (dayl). With its observation-based design and high spatial resolution, the Daymet dataset is well-suited for analyzing long-term climate variability and heat extremes in Texas. For this study, we extracted Daymet daily records covering the period 1980–2023 for Tmax and Tmin variables, and average daily temperature (T), used for the computation of EHF, was computed as the average of daily Tmax and Tmin of the day. The relative humidity (RH) was derived using vapour pressure and temperature data (Chegini et al., 2021). The data was projected from its original coordinate system (Lambert Conformal Conic) to the geographic coordinate system and the results were spatially aggregated to the county level by overlaying county boundaries and computing area-weighted averages across grid cells within each county. This procedure ensured consistency between the high-resolution gridded product and the administrative boundaries relevant for impact assessment. The demographic (age group wise population) of Texas counties for year 2020 was obtained from U.S. Census Bureau (U.S. Census Bureau, 2023). The per capita income (PCI), percentage population below poverty (PPBP), percentage of outdoor workers (POW), and percentage population with health insurance (PPWI) datasets were obtained from American Community Survey estimates (U.S. Census Bureau, U.S. Department of Commerce, 2024a, 2024b, 2024c, 2024d).

#### 3.2 Excess Heat Factor

EHF is a widely used metric for identifying and characterizing heatwaves, which integrates two key components, Excess Heat Index Significance (EHIsig) and Excess Heat Index Acclimatization (EHIaccl), both of which are strongly linked to human heat stress and health impacts (Nairn et al., 2009; Nairn & Fawcett, 2013). EHIsig, defined as the difference between the 3-day mean temperature and the 90th percentile of a long-term reference period, captures the long-term heat anomaly. In contrast, EHIaccl, derived from the difference between the 3-day mean temperature and the mean temperature of the preceding 30 days, reflects short-term heat anomaly and acclimatization effects. In this study, data from a fixed baseline period (1980 - 1990) was used to define the reference climatology. The EHF for each day was computed using the following formulas:

$$EHF(d) = EHI_{sig}(d) \times \max [1, EHI_{accl}(d)] \quad \dots(i)$$

$$EHI_{sig}(d) = \bar{T}_3(d) - T_{90}(d) \quad \dots(ii)$$

$$EHI_{accl}(d) = \bar{T}_3(d) - \bar{T}_{30}(d) \quad \dots(ii)$$

Where,  $\bar{T}_3(d)$  is 3-day mean temperature [  $\bar{T}_3(d) = \frac{1}{3} \sum_{i=0}^2 T_{d-i}$  ],  $\bar{T}_{30}(d)$  is 30-day antecedent mean temperature [  $\bar{T}_{30}(d) = \frac{1}{30} \sum_{i=1}^{30} T_{d-i}$  ], and  $T_{90}(d)$  is 90<sup>th</sup> percentile climatology  $T_{90}(d)$  of average daily temperature (i.e., non-time-varying climatology for base period). A 31-day moving window ( $\pm 15$  days) centered on each calendar day was used to derive the reference climatology during the baseline period. A positive EHF value indicates the occurrence of a heatwave, and its magnitude reflects the intensity of the event. Because EHF is derived from the product of the long-term and the short-term anomalies, the index increases quadratically as thermal conditions become more extreme. The EHF is intrinsically a localized index, as both its components are derived from the historical temperature characteristics of the same location. Consequently, regions with greater temperature variability tend to exhibit higher EHF values, whereas areas with narrower temperature ranges produce smaller values.

### 3.3 Heatwave Characteristics

This study examines long-term heatwave characteristics during the period 1980–2023 using EHF. A heatwave day was identified when EHF(d) exceeds 0, and consecutive runs of at least three such days were classified as heatwave events (Perkins & Alexander, 2013). For each heatwave event, the start and end dates were extracted, and the duration, maximum and mean EHF intensity, and the mean and peak temperatures during the heatwave events were computed. The heatwave analysis was done for entire year rather than a particular season. The heatwave characteristics, presented in Table 1, were aggregated at annual time-scale and classified into three key categories, frequency, duration, and intensity. Additionally, the day of first heatwave (HWT) was derived as an indicator for detecting shifts in heatwave onset. Further, heatwave indicators were aggregated across the state and counties, and the mean values were analysed and discussed. To assess long-term changes in heatwave characteristics, the Modified Mann–Kendall (MMK) test (Hamed & Rao, 1998) was applied to detect monotonic trend, and significance was evaluated at the 5% level. Moreover, Sen’s slope estimator (Sen, 1968) was applied to quantify the magnitude of change. To compute the EHF and associated heatwave characteristics, the dargueso/EHF v2.2 Python package (Argüeso, 2024) was used, while temporal trends were assessed with the pyMannKendall library (Hussain and Mahmud, 2019).

Table 1: Heatwave indicators applied in this study

S/N	Indicator	Definition	Unit	Category
1	Number of Heatwaves (HWN)	Number of individual heatwave events per year. A heatwave event was defined as a period of at least three consecutive days during which EHF values exceeded zero.	-	Frequency

2	Heatwave days Frequency (HWF)	The total number of days contributing to heatwave events in a year, as identified through HWN.	days	Frequency
3	Mean duration of Heatwaves (HWL)	The average duration of heatwave events calculated across all heatwaves occurring within a given year.	days	Duration
4	Annual Maximum Heatwave Duration (HWD)	The maximum uninterrupted heatwave duration within a given year, as determined by HWN.	days	Duration
5	annual Mean Heatwave Magnitude (HWM)	The average intensity of heatwave events detected by HWN within a given year.	$^{\circ}\text{C}^2$	Intensity
6	annual Maximum Heatwave Amplitude (HWA)	The maximum heatwave magnitude observed across heatwave events within a given year.	$^{\circ}\text{C}^2$	Intensity
7	annual Mean Heatwave Temperature (HWMt)	The mean temperature associated with all heatwave events within a year.	$^{\circ}\text{C}$	Temperature
8	annual Maximum Heatwave Temperature (HWAt)	The temperature corresponding to the day on which the annual maximum heatwave amplitude occurred within a year.	$^{\circ}\text{C}$	Temperature
9	Timing of first Heatwave (HWT)	The onset day of the first heatwave event within each year, quantified as the number of days from the start of January to the beginning of the earliest heatwave.	day	Onset shift

### 3.4 Heatwave Vulnerability Index

The Heatwave Vulnerability Index (HVI) was developed by combining information on heatwave hazard, vulnerable population, and adaptive capacity represented by per-capita income. Heatwave hazard was represented using six indicators that describe different aspects (frequency, duration and severity) of heatwaves. These indicators include HWN HWF, HWL, HWD, and two severity measures derived from HWM and HWA. The first four indicators capture the frequency and duration of heatwaves, whereas HWM and HWA represent the thermal intensity of heatwave events (Table 1). Literature suggests that the heatwave intensity reflect regional climatology (Nairn et al. 2018), hence cannot be directly compared across regions. To overcome this limitation, EHF-based severity concept was introduced, where intensity values are normalized using a high threshold of EHF (85<sup>th</sup> percentile of positive EHF values, denoted as EHF85p) that represents the upper range of the local climatology (Oliveira et al., 2022). This approach yields a dimensionless severity index that reflect how anomalous a heatwave is relative to its own climatology rather than

to absolute temperature values. Following this conceptual basis, the present study applied the same normalization strategy to HWM and HWA to compute regionally comparable indicators of heatwave severity [  $HWMS = \frac{HWM}{EHF85p}$  , and  $HWAS = \frac{HWA}{EHF85p}$  ]. For the heatwave vulnerability assessment, the six hazard indicators (HWN, HWF, HWL, HWD, HWMS, and HWAS) and RH were derived for each Texas county by averaging their values in space and time for most recent ten-year period (from 2014 to 2023 in this study). Since heatwave indicators differ in magnitude and statistical behaviour, each was transformed to a common zero-to-one scale using the cumulative distribution function of its best-fitting probability distribution. For any indicator  $X$ , the normalized score was obtained using  $X^* = F_X(X)$ , where  $F_X$  denotes the fitted cumulative distribution function. The Composite Heatwave Indicator (CHI) was then computed as the geometric mean of the six normalized hazard measures, expressed through:

$$CHI = (X_{HWN}^* \cdot X_{HWF}^* \cdot X_{HWL}^* \cdot X_{HWD}^* \cdot X_{HWMS}^* \cdot X_{HWAS}^* \cdot X_{RH}^*)^{1/7} \quad \dots(iv)$$

Heat-related health risks are known to be higher among older adults, and vulnerability studies therefore commonly include this demographic as an indicator of sensitivity to extreme heat (Tomlinson et al., 2011; Williams et al., 2012; Wolf & McGregor, 2013; Hatvani-Kovacs et al., 2016). In the present study, the vulnerable population was therefore represented by the number of individuals aged sixty-five years and older, combined with infants younger than five years who are also physiologically susceptible to heat stress. The distribution of the vulnerable population (POP) across Texas counties was highly skewed, reflecting substantial variations in county size and demographic composition. To reduce this skewness and improve comparability across counties, a logarithmic transformation was applied, and the transformed values were then normalised to a zero-to-one range by dividing each value by the maximum transformed value observed across the state [  $nPOP = \frac{\log(POP)}{\max(\log(POP))}$  ]. Similarly, PPBP and POW were normalized [  $nPPBP = \frac{\log(PPBP)}{\max(\log(PPBP))}$ ;  $nPOW = \frac{\log(POW)}{\max(\log(POW))}$  ] to include them in computation of overall exposure. The overall exposure (EXPS) was then computed as the geometric mean of nPOP, nPPBP, and nPOW).

Adaptive capacity (AC) forms another key dimension of heatwave vulnerability, as demographic sensitivity alone does not fully determine community risk. Economic resources play a central role in shaping the ability of populations to anticipate, withstand, and recover from extreme heat. Per-capita income (PCI) therefore serves as a practical proxy for the economic capacity of a community to respond to heat stress, influencing access to cooling technologies, healthcare, housing quality, and other protective measures. Similar to POP, county-level PCI has also been transformed and normalized [  $nPCI = \frac{\log(PCI)}{\max(\log(PCI))}$  ]. The PPWI is another indicator of AC as it reflects access to healthcare. Similar to PCI, it has been normalized using a logarithmic transformation [  $nPPWI = \frac{\log(PPWI)}{\max(\log(PPWI))}$  ] to compute the overall AC. The AC was then computed as the geometric mean of nPCI and nPPWI.

The HVI was then computed using a multiplicative formulation that combines heatwave hazard (CHI), vulnerable population (nPOP), and adaptive capacity (nPCI) in a proportional manner. The index was expressed as:

$$HVI = \frac{CHI \times EXPS}{AC} \dots(v)$$

Higher HVI values signal greater vulnerability of counties to heatwaves, arising from the combined effects of severe heatwave conditions, larger vulnerable populations, and limited adaptive capacity.

## 4 Results

### 4.1 Heatwave Frequency

In this study, the frequency of heatwaves was characterized by number of heatwave events (HWN) and heatwave days (HWF). The decadal maps of HWN reveal a clear intensification and spatial expansion of extreme heat events across Texas from 1980 to 2023 (Figure 2a, c, d, e, f). In the 1980s, heatwaves were relatively rare and spatially uniform (Figure 2a) with all 254 counties experiencing less than five events per year. During the 1990s, a modest increase was observed, particularly in West Texas (the El Paso region) and southern state counties (Figure 2c), although much of the state remained in the low-frequency range. A marked escalation occurred in the 2000s, when hotspots of higher HWN emerged in West, South, and Northeast Texas (Figure 2d), with 15 counties experiencing more than 7 heatwave events. The 2010s exhibited a more widespread intensification, as South and West Texas, along with coastal and central regions (Figure 2e), recorded more than 7 events in 100 counties. By the 2020s, the HWN had reached unprecedented levels, with 233 and 35 counties of Texas experienced more than 7 and 10 events respectively (Figure 2f). On average, state-level statistics confirm the gradual increase in HWN, with average value increased from ~3.6 events in the 1980s to ~4.5 in the 1990s, and then ~5.7 in the 2000s (Figure 2b). The trend intensified further in the 2010s, reaching ~7 events, and accelerated markedly in the early 2020s, with a statewide average of ~9 events per year (Figure 2b), despite the decade being incomplete. This represents an overall 147% increase in HWN since the 1980s, underscoring the rapid escalation of heat stress across Texas. Trend analysis using the Z statistic of MMK test and Sen's slope estimator highlights the statistically significant increase in HWN across Texas over the 1980–2023 period (Figure 2g, i). The results show that all 254 counties exhibit positive Z-MMK values (at the 95% confidence level), with a statewide mean of 3.67 and a median of 3.45 (Figure 2h), well above the significance threshold ( $|Z| > 1.96$  at the 95% confidence level). Overall, 247 (97%) counties of Texas show statistically significant positive trends. The corresponding Sen's slope estimates confirm this acceleration (Figure 2i), with a statewide mean of 0.12 (median=0.11) events per year, approximately one additional heatwave per decade (Figure 2h). In some counties (such as Culberson, Jeff Davis, Hudspeth, and Brewster counties), particularly in West Texas, the lower Rio Grande Valley (which shares border with Mexico), and along the Gulf Coast, which are also among the most socio-economically vulnerable

regions of the state, slopes exceed 0.20 events per year (Figure 2i). Together, these findings provide robust evidence that number of heatwave events in Texas are increasing as well as accelerating at a rate that poses mounting risks. Notably, the spatial heterogeneity of slope magnitudes underscores the need for region-specific adaptation strategies.

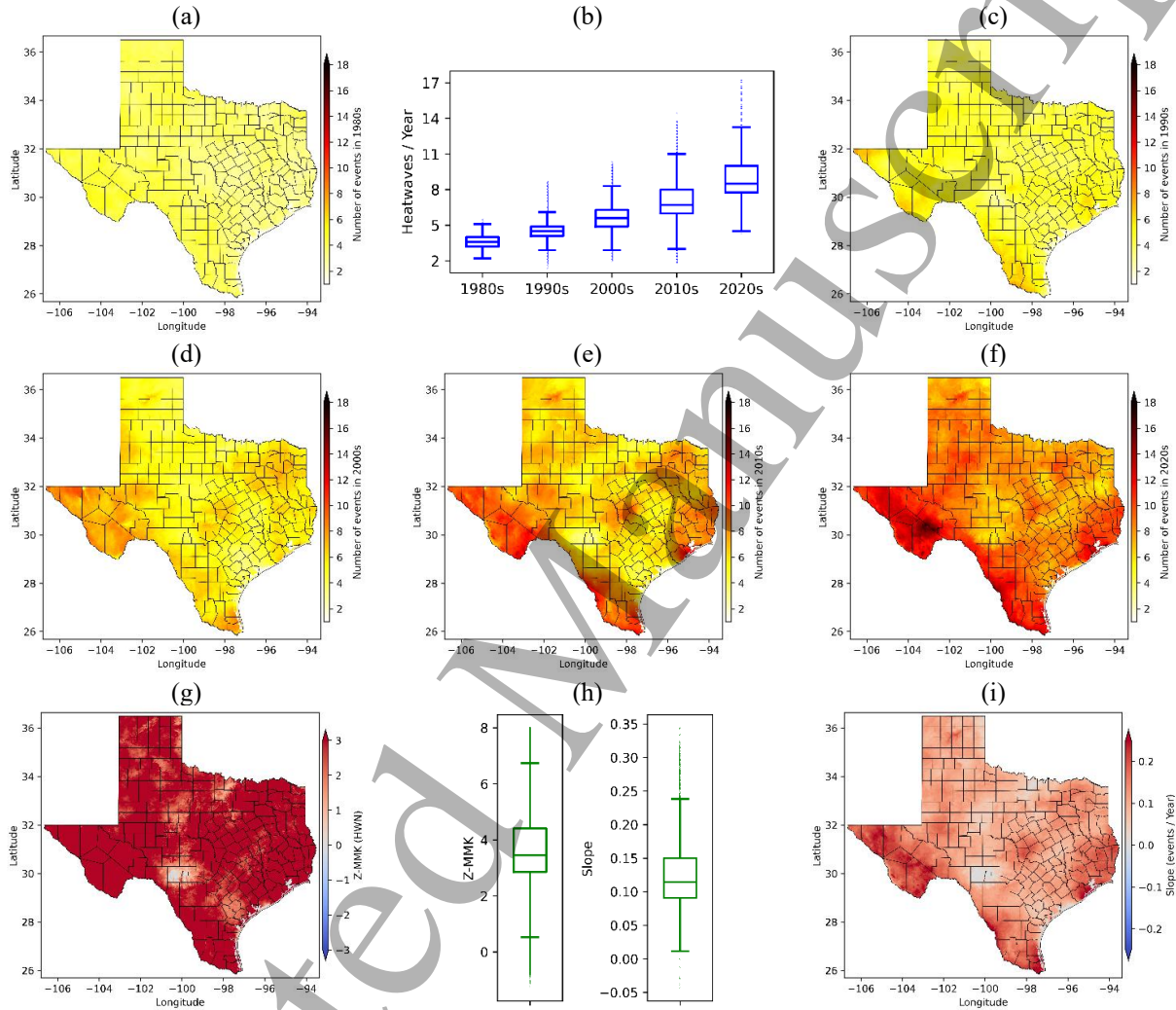
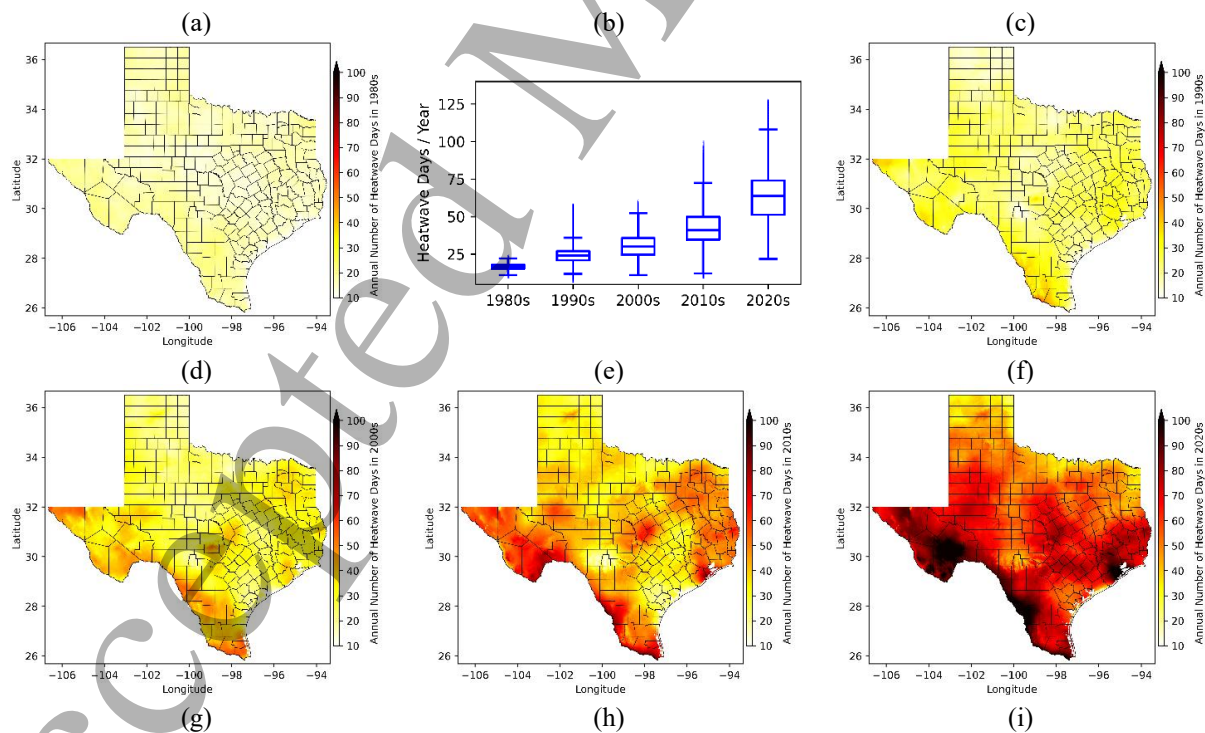


Figure 2: Spatiotemporal variability in the number of heatwave events in a year (HWN) across the 1980s, 1990s, 2000s, 2010s, and 2020s (subplots a, c, d, e, and f, respectively); statistical summary of HWN shown as a boxplot (subplot b); Z-values from the MMK trend test (subplot g) and Sen's slope of the trend in HWN during 1980 to 2023 (subplot i); statistical summaries of the Z-values and Sen's slope presented as boxplot (subplot h)

The spatiotemporal evolution of HWF across Texas reveals an upward trajectory from the 1980s through the 2020s, both in terms of magnitude and spatial coverage (Figure 3a, c, d, e, f). In the 1980s, the state experienced relatively few heatwave days (Figure 3a), with range 9–25 days and averages around 16 days annually (Figure 3b). The spatial distribution was fairly uniform, and no region exhibited exceptionally high HWF (Figure 3a). By the 1990s, the statewide mean increased to nearly 24 days (Figure 3b), and early signs of spatial heterogeneity in HWF was observed over

south and west Texas (Figure 3c). The 2000s marked a further intensification, with the statewide mean climbing to about 30 days (Figure 3b) and 18 counties exceeding 40 days annually (Figure 3d). In the 2010s, heatwaves became a widespread climatic hazard (Figure 3e), with the mean HWF reached 41 days statewide (Figure 3b), and 46 counties reported above 50 heatwave days per year. Hotspots became more apparent in the east, south, west and some parts of central Texas, and Rio Grande valley, bordering with Mexico (Figure 3e). The escalation is most pronounced in the 2020s, with a statewide mean surpassing 60 days (Figure 3b), and extremes exceeding 90 days in 5 counties (Zapata, Maverick, Brewster, Webb, and Galveston), that is one in approximately every 4 days of the year. Spatial map shows comparatively higher HWF over west Texas, the Rio Grande Valley, and coastal regions (Figure 3f). Even northern parts of Texas, which was historically less affected, recorded substantial increases relative to 1980s (Figure 3f). The MMK test and Sen's slope further substantiate the intensification of HWF across Texas (Figure 3g, i). The map (Figure 3g) indicate widespread increasing trends, with 250 counties exhibiting statistically significant changes. Among these, 54 counties show trend slopes exceeding 10 days per decade (Figure 3i). Hotspots of higher HWF trend slope were observed primarily in west Texas, south Texas, the Rio Grande Valley, and the coastal regions (Figure 3i). In contrast, a slope of less than 5 days/decade was observed over 30 counties, and in 4 counties (Edwards, Real, Montague, and Lipscomb) the slope was less than 3 days/decade (Figure 3i). The boxplot (Figure 3h) indicates a median HWF trend slope of approximately 8 days per decade across Texas.



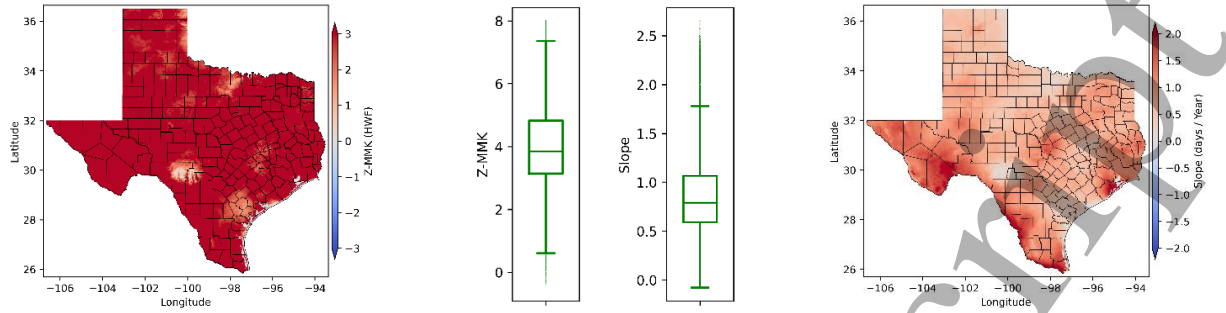


Figure 3: Spatiotemporal variability in the number of heatwave days in a year (HWF) across the 1980s, 1990s, 2000s, 2010s, and 2020s (subplots a, c, d, e, and f, respectively); statistical summary of HWF shown as a boxplot (subplot b); Z-values from the MMK trend test (subplot g) and Sen's slope of the trend in HWF during 1980 to 2023 (subplot i); statistical summaries of the Z-values and Sen's slope presented as boxplot (subplot h)

## 4.2 Heatwave Duration

The analysis of heatwave duration focused on two important metrics, the mean duration of heatwave events (HWL) and the duration of the longest heatwave of the year (HWD). The results reveal temporal intensification and spatial heterogeneity of HWL across Texas (Figure 4). The decadal maps (Figure 4a, c, d, e, f) indicate that HWL increased steadily from the 1980s through the 2020s. The average HWL, which was around 4.5 days in the 1980s, lengthened to approximately 6.8 days by the 2020s (Figure 4b). This shift demonstrates that heatwaves are no longer short-lived anomalies but persist longer, exposing populations and ecosystems to sustained thermal stress. In the 1980s, the HWL was relatively lower across much of Texas (Figure 4a), with hotspots in 38 counties (e.g. Lavaca, Nacogdoches, Victoria, Wharton, Jackson etc.) where HWL was higher than 5 days. By the 2000s, the spatial footprint of prolonged heatwaves expanded, particularly in south Texas (Figure 4d). In 2010s, the higher HWL values expanded further in north-west directions (Figure 4e). By the 2020s, nearly the entire state (except northern areas) was affected by longer heatwaves (Figure 4f), with average HWL exceeding 8 days over 34 counties. This decadal increase underscores a shift from localized hotspots to widespread, statewide persistence of longer heatwave events. The trend analysis confirms a statistically significant increase in HWL over 184 counties of Texas over the past four decades (Figure 4g). The boxplot reveal that the average slope of trend in HWL is about 0.5 days/decade (Figure 4h), and over 6 counties (Galveston, Brewster, Val Verde, Terrell, Gillespie, and Maverick), slope exceeded 0.8 days/decade. Overall, the higher slope of HWL trend was observed over Rio Grande valley, and some parts of central and coastal region (Figure 4i). Only a few localized pockets, primarily in 6 coastal and southeastern counties (Refugio, San Patricio, Aransas, Goliad, Calhoun, and Bee), exhibited neutral or weakly negative slopes (Figure 4i).

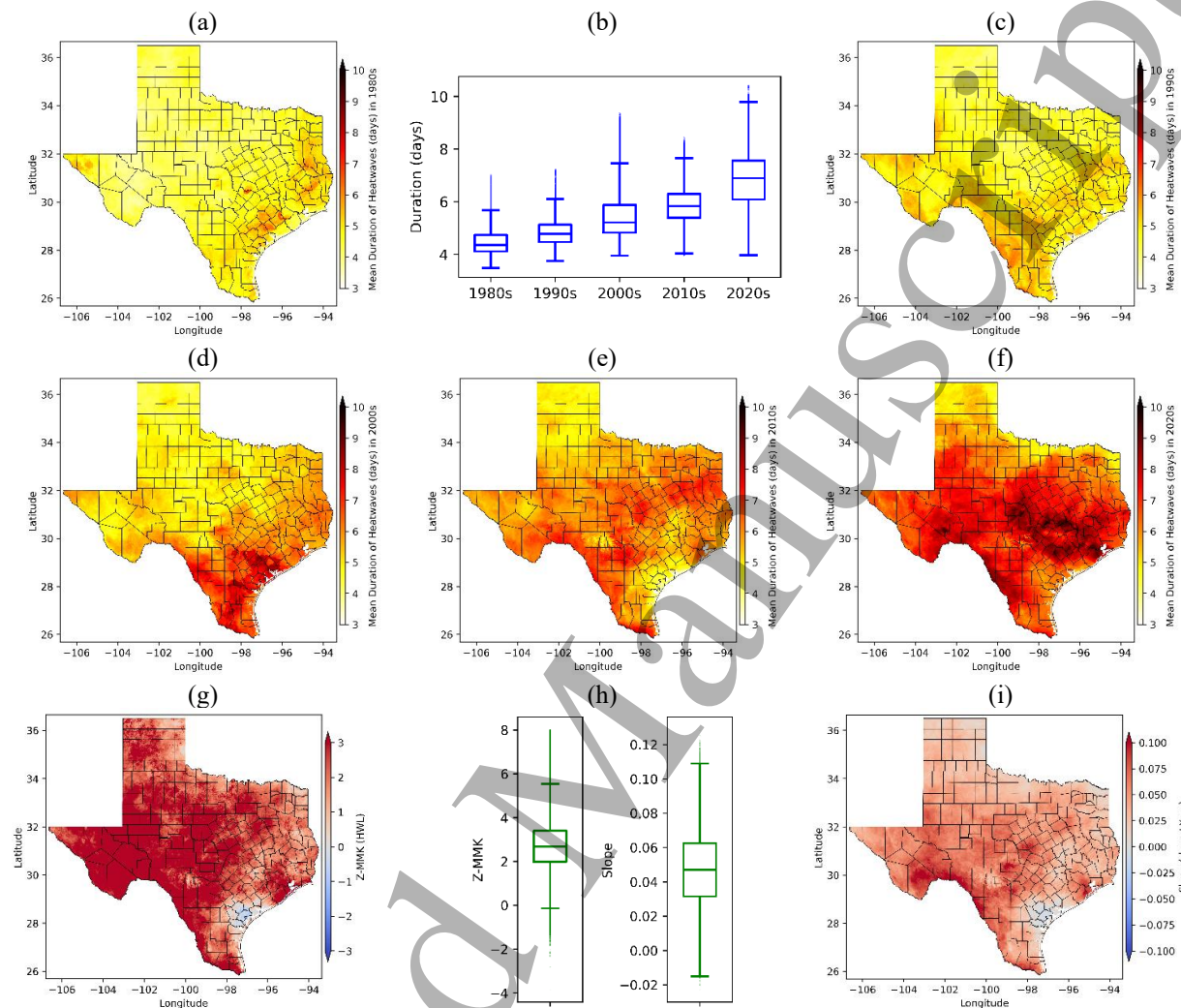
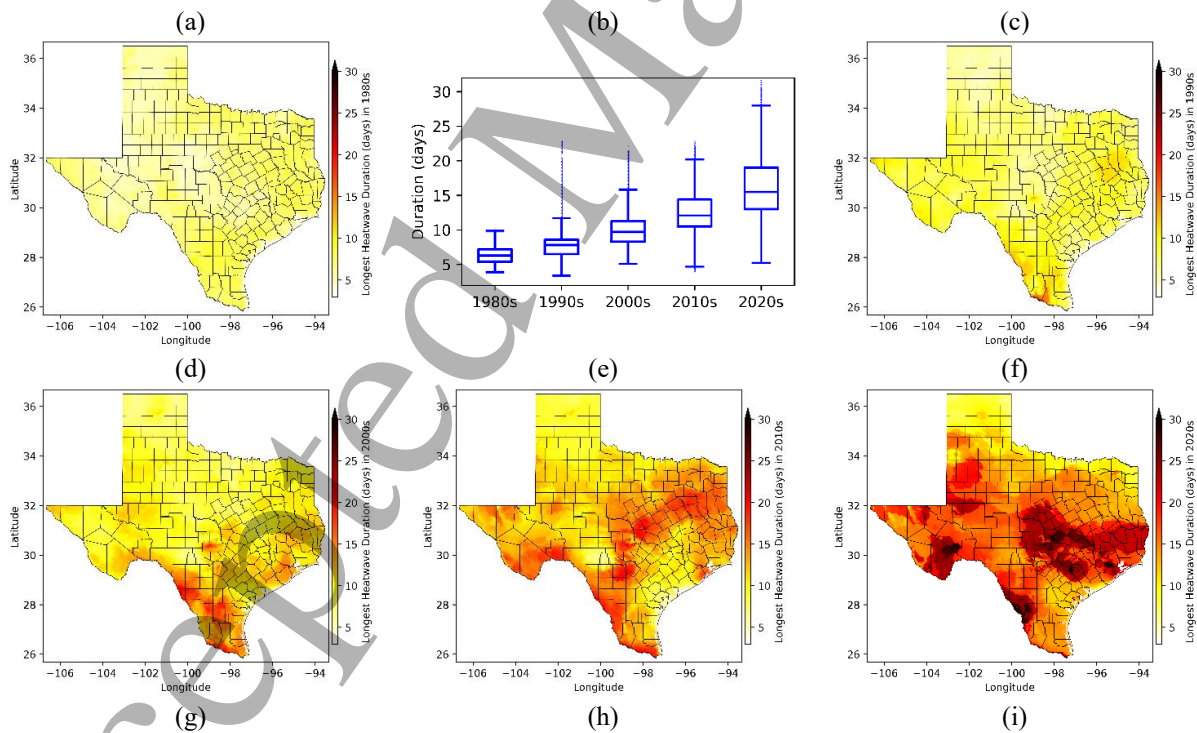


Figure 4: Spatiotemporal variability in the mean duration of heatwave events (HWL) across the 1980s, 1990s, 2000s, 2010s, and 2020s (subplots a, c, d, e, and f, respectively); statistical summary of HWL shown as a boxplot (subplot b); Z-values from the MMK trend test (subplot g) and Sen's slope of the trend in HWL during 1980 to 2023 (subplot i); statistical summaries of the Z-values and Sen's slope presented as boxplot (subplot h)

Similar to HWL, the temporal dynamics of the HWD across Texas demonstrates a clear and increasing trend since the 1980s (Figure 5). During the 1980s, the longest heatwaves were relatively short-lived, with a statewide average HWD of 6.3 days, and limited spatial variability across the state (Figure 5a, b). In the 1990s, the average HWD increased to 7.7 days (Figure 5b), with 14 counties experiencing extreme values exceeding 10 days. These counties, such as Starr, Hidalgo, Brooks, Cherokee, Webb, and Houston, emerged as hotspots in southern and eastern Texas, indicating the onset of more regionally concentrated heatwave risks (Figure 5c). In the 2000s, the average HWD increased further to nearly 10 days (Figure 5b), with five counties, Zavala, Jim Wells, Duval, Dimmit, and Maverick, recording extreme durations exceeding 15 days.

These hotspots were primarily concentrated in the lower Rio Grande Valley and coastal regions (Figure 5d). By the 2010s, the average HWD had increased further to 12.5 days (Figure 5b), with hotspots shifting into eastern and central Texas, including parts of the Rio Grande Valley (Figure 5e). Moreover, 10 counties experienced extreme durations exceeding 17 days. In 2020s, a significant increase in HWD occurred, with average HWD surged to 16.3 days (Figure 5b), nearly tripling the levels of the 1980s. Prolonged heatwaves lasting more than 20 days were recorded in 51 counties (Figure 5f), and 5 of these counties (Lavaca, Burnet, Milam, Burleson, and Williamson) exhibited average HWD values greater than 25 days. The MMK trend test and Sen's slope estimator provide strong evidence that the longest heatwave duration in Texas has increased over the study period (Figure 5g, i). The trend analysis reveals that 239 counties exhibit significant positive trends (Figure 5g), with a statewide mean slope of 1.7 days/decade (Figure 5h). Hotspots of higher slopes are particularly evident over the Rio Grande valley, western, central, and eastern Texas (Figure 5i), with 26 counties (including Webb, Terrell, Burnet, Brewster, Gillespie, Maverick) having average slope of higher than 2.5 days/decade. The spatial heterogeneity of slope magnitudes (Figure 5i) highlights regions of acute vulnerability, which are also characterized by higher baseline temperatures and humidity, suggesting that compound heat stress risks will likely become more severe.



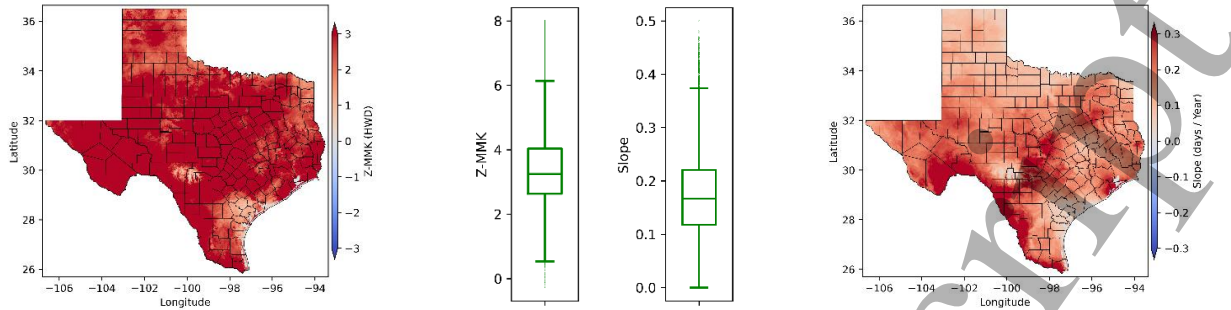


Figure 5: Spatiotemporal variability in the duration of the longest heatwave of the year (HWD) across the 1980s, 1990s, 2000s, 2010s, and 2020s (subplots a, c, d, e, and f, respectively); statistical summary of HWD shown as a boxplot (subplot b); Z-values from the MMK trend test (subplot g) and Sen's slope of the trend in HWD during 1980 to 2023 (subplot i); statistical summaries of the Z-values and Sen's slope presented as boxplot (subplot h)

### 4.3 Heatwave Intensity

In this study, the intensity of heatwaves was characterized by mean intensity (HWM) and annual maximum intensity (HWA). The decadal evolution and trend analysis results of HWM and HWA are presented in Figure 6 and 7, respectively. The findings indicate a clear long-term changes in HWM, with decadal fluctuations across Texas (Figure 6a, b, c, d, e, f). The average HWM across Texas (Figure 6b) exhibited an increasing trajectory from  $5.2\text{ }^{\circ}\text{C}^2$  in the 1980s to a peak of  $7.1\text{ }^{\circ}\text{C}^2$  in the 2000s, after which it declined to  $5.7\text{ }^{\circ}\text{C}^2$  in the 2010s and subsequently increased again to  $6.9\text{ }^{\circ}\text{C}^2$  in the 2020s. Relative to the 1980s, this represents a 32% increase in the 2020s, with 193 counties exhibiting an increase of at least  $1\text{ }^{\circ}\text{C}^2$  and 6 counties (Callahan, Irion, Tarrant, Parker, Eastland, and Palo Pinto) even experiencing increases of more than  $4\text{ }^{\circ}\text{C}^2$ . Spatial maps show that the northeast quadrant of Texas has been the persistent hotspot across decades (Figure 6a, c, d, e, f). Counties such as Marion, Harrison, Cass, and Upshur recorded the highest average HWM, exceeding  $11\text{ }^{\circ}\text{C}^2$  in 2020s. In contrast, west and south-coastal Texas (e.g., El Paso, Hudspeth, Presidio, Real, Cameron, Edwards, Brewster, Bailey, AND Culberson Counties) recorded lowest intensities in 2020s (Figure 6f), with average HWN values below  $5\text{ }^{\circ}\text{C}^2$ . Trend analysis reveals that 229 counties exhibit increasing trends, of which 30 show statistically significant increases at the 95% confidence level (Figure 6g). In contrast, 25 counties display negative trends, though none of them are statistically significant. The average slope across the state is about  $0.4\text{ }^{\circ}\text{C}^2/\text{decade}$  (Figure 6h), with higher slopes observed across west, north-central and north-east Texas (Figure 6i). Notably, 8 counties (Midland, Stephens, Glasscock, Irion, Parker, Wise, Jack, and Palo Pinto) exhibited slopes exceeding  $0.8\text{ }^{\circ}\text{C}^2$  per decade. Conversely, 5 counties (Newton, Jasper, Sabine, Tyler, and San Augustine) exhibited negative slopes below  $-0.3\text{ }^{\circ}\text{C}^2/\text{decade}$ , possibly reflecting microclimatic moderation associated with extensive water bodies within these counties.

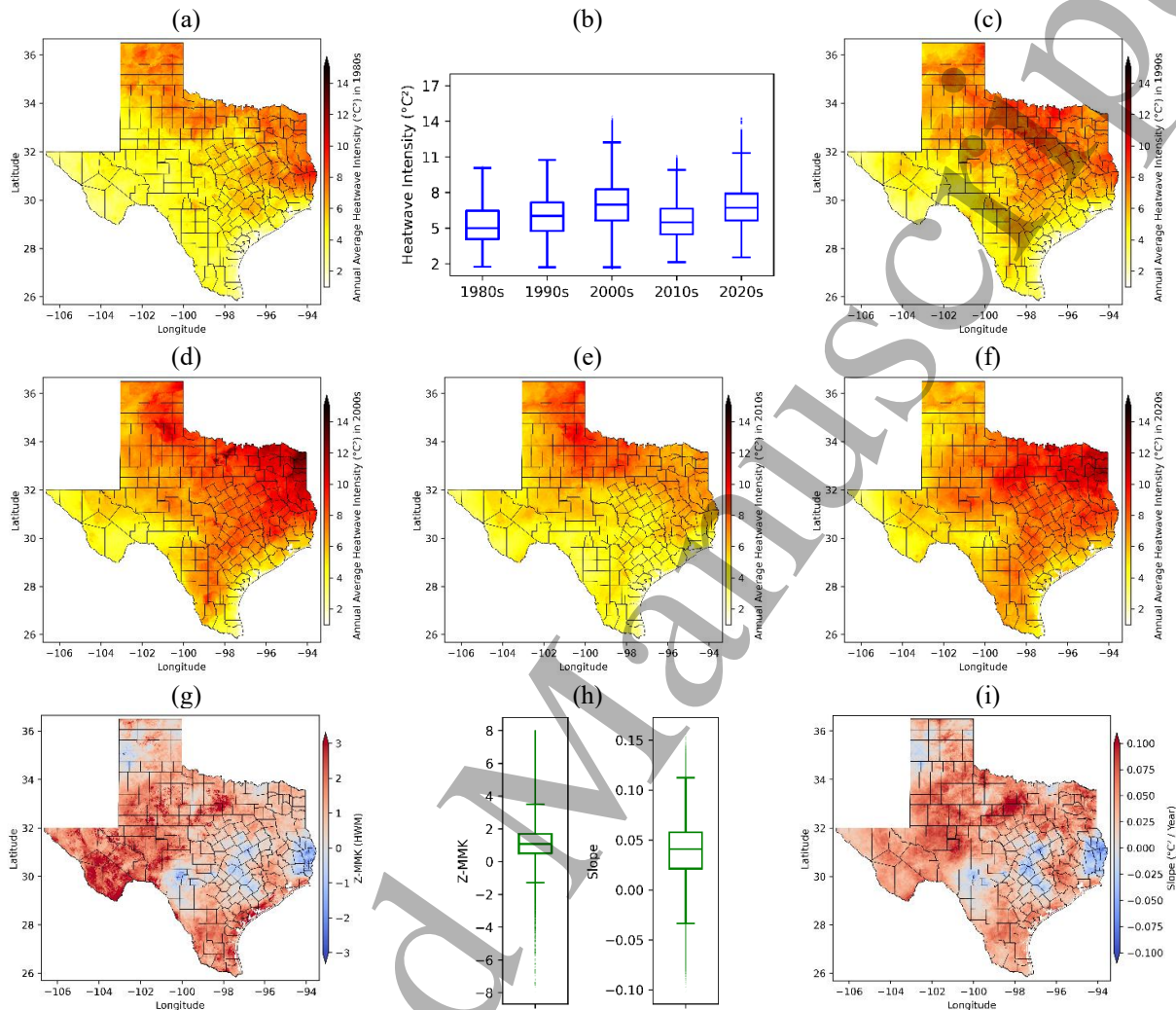
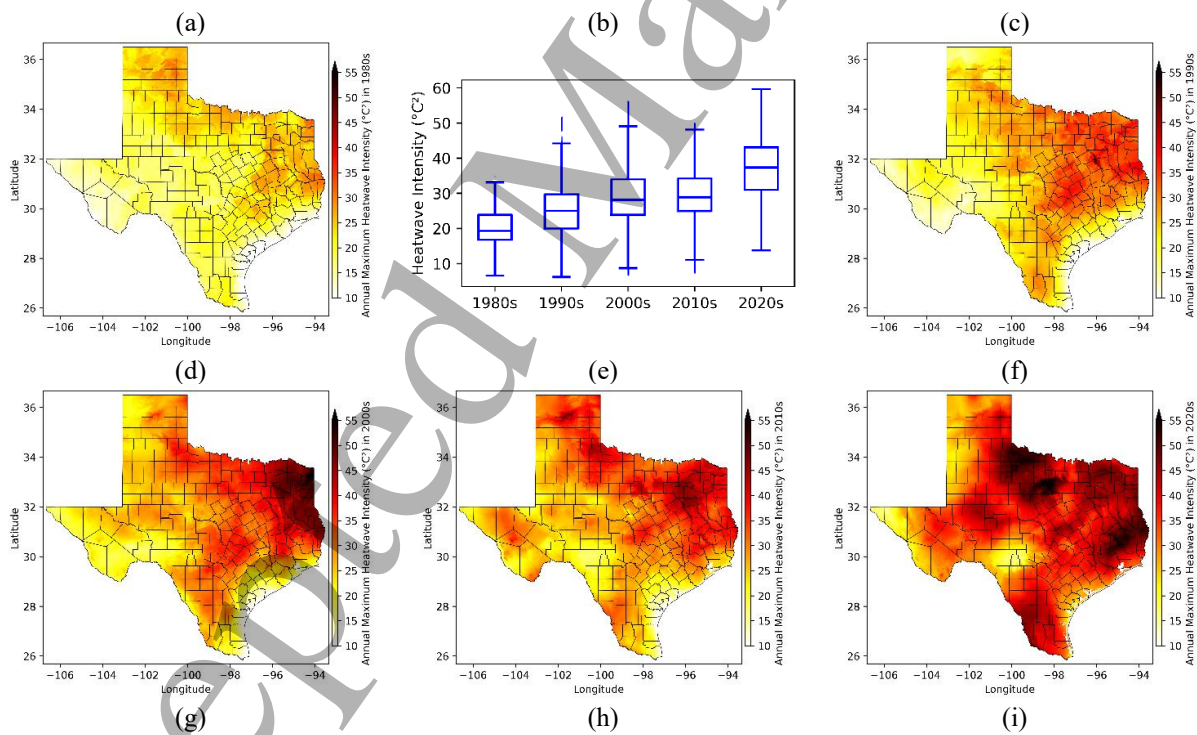


Figure 6: Spatiotemporal variability in the mean intensity of heatwaves in a year (HWM) across the 1980s, 1990s, 2000s, 2010s, and 2020s (subplots a, c, d, e, and f, respectively); statistical summary of HWM shown as a boxplot (subplot b); Z-values from the MMK trend test (subplot g) and Sen's slope of the trend in HWM during 1980 to 2023 (subplot i); statistical summaries of the Z-values and Sen's slope presented as boxplot (subplot h)

Similar to HWM, Texas has experienced a clear, statewide intensification of HWA over the last four decades (Figure 7). The statewide average HWA (Figure 7b) rises from  $\sim 20$   $^{\circ}\text{C}^2$  in the 1980s to  $\sim 25$   $^{\circ}\text{C}^2$  in the 1990s,  $\sim 29$   $^{\circ}\text{C}^2$  in the 2000s, holds near  $\sim 30$   $^{\circ}\text{C}^2$  in the 2010s, and then steps up sharply to  $\sim 37$   $^{\circ}\text{C}^2$  in the 2020s, an increase of  $\sim 83\%$  relative to the 1980s baseline. Notably, the lower tail also rises significantly, indicating that even historically cooler counties now face higher peak heatwave intensity. The interquartile range widens from 7  $^{\circ}\text{C}^2$  to 12  $^{\circ}\text{C}^2$ , signaling growing spatial disparities across counties. In the 1980s, HWA is relatively low across most of the state, with only modest pockets of higher HWA (Figure 7a). By the 1990s, a higher HWA hotspots appear across east and northeast Texas, extending into parts of central Texas (Figure 7c), a first sign that

high-intensity peaks are no longer localized. The 2000s exhibit a marked intensification along the northeast corridor and parts of the north-central region (Figure 7d), with 68 and 32 counties recording HWA values exceeding  $35\text{ }^{\circ}\text{C}^2$  and  $40\text{ }^{\circ}\text{C}^2$ , respectively. The 2010s maintain widespread elevated values (Figure 7e), with 25 counties recording HWA values exceeding  $40\text{ }^{\circ}\text{C}^2$ . The 2020s map shows a markedly different pattern, with higher HWA becoming widespread across north, northeast, east, and central Texas, and elevated values extending toward the Gulf Coast and the Lower Rio Grande Valley (Figure 7f). Overall, 53 counties recorded HWA values exceeding  $45\text{ }^{\circ}\text{C}^2$ . The Z-MMK values provides statistical confirmation that Texas has experienced an increase in HWA (Figure 7g), with 170 counties exhibiting statistically significant increasing trends. The trend slopes indicate an average increase of  $4.5\text{ }^{\circ}\text{C}^2/\text{decade}$  (Figure 7h), with 44 counties exhibiting average slopes greater than  $6\text{ }^{\circ}\text{C}^2/\text{decade}$  (Figure 7i). Counties such as Polk, Hopkins, Trinity, Red River, Delta, Upshur, Palo Pinto, Cottle, Hardeman, and Foard recorded average slopes greater than  $7\text{ }^{\circ}\text{C}^2/\text{decade}$ . This consistent positive trend across nearly the entire state underscores that the intensification of heatwave peaks is not a localized phenomenon but a widespread climatic shift. West Texas and the Panhandle, though historically less intense in terms of peak intensity, now exhibit a clear increasing trend, reflecting the diffusion of intensification into semi-arid regions.



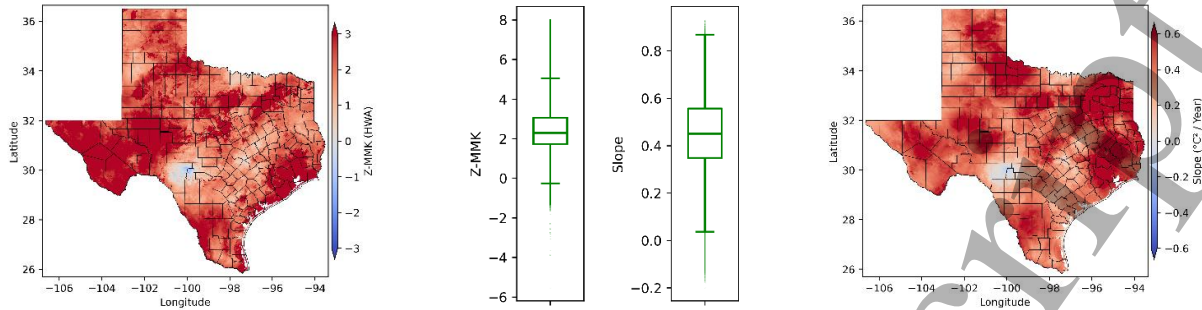


Figure 7: Spatiotemporal variability in the maximum intensity of heatwaves in a year (HWA) across the 1980s, 1990s, 2000s, 2010s, and 2020s (subplots a, c, d, e, and f, respectively); statistical summary of HWA shown as a boxplot (subplot b); Z-values from the MMK trend test (subplot g) and Sen's slope of the trend in HWA during 1980 to 2023 (subplot i); statistical summaries of the Z-values and Sen's slope presented as boxplot (subplot h)

#### 4.4 Heatwave Temperature

The temperature of heatwaves was assessed in terms of mean temperature of heatwaves (HWMt) and temperature corresponding to peak heatwave intensity (HWAt). Texas exhibits a persistent spatial gradient in HWMt across all decades, with the warmest heatwave days concentrated in the Lower Rio Grande valley and Coastal region and progressively cooler conditions toward the Panhandle and west Texas (Figure 8a, c, d, e, f). In the 1980s, 24 counties exhibited average HWMt values exceeding 27 °C, including five counties, Zapata, Jim Hogg, Starr, Brooks, and Hidalgo, where the averages surpassed 28 °C (Figure 8a). In contrast, 11 counties recorded average HWMt values below 20 °C. This spatial pattern persists across decades (Figure 8c, d, e, f), while no county exhibits an average HWMt below 20 °C, the statewide mean remains nearly constant at about 24 °C (Figure 8b), and only 3 counties (Zapata, Starr, and Hidalgo) register values exceeding 28 °C. The Z-MMK results (Figure 8g) indicate that only nine counties, Oldham, Franklin, Sutton, Hopkins, Anderson, Somervell, Cherokee, Bosque, and Delta, exhibit a statistically significant increasing trend in HWMt. In contrast, although 22 counties (including Aransas, Refugio, Calhoun, Matagorda, San Patricio, and Nueces) show negative Z-MMK values, none of them are statistically significant. The average trend slope across the state is 0.3°C/decade (Figure 8h), with 21 counties exceeding 0.6°C/decade and seven counties, Sherman, Oldham, Wichita, Hall, Moore, Bosque, and Somervell, exceeding 0.8°C/decade. The higher trend slopes are particularly concentrated over the Panhandle, north Texas, and parts of central Texas (Figure 8i). This represents a marked transition for historically cooler regions of the High Plains, which are now emerging as new hotspots of warmer heatwave.

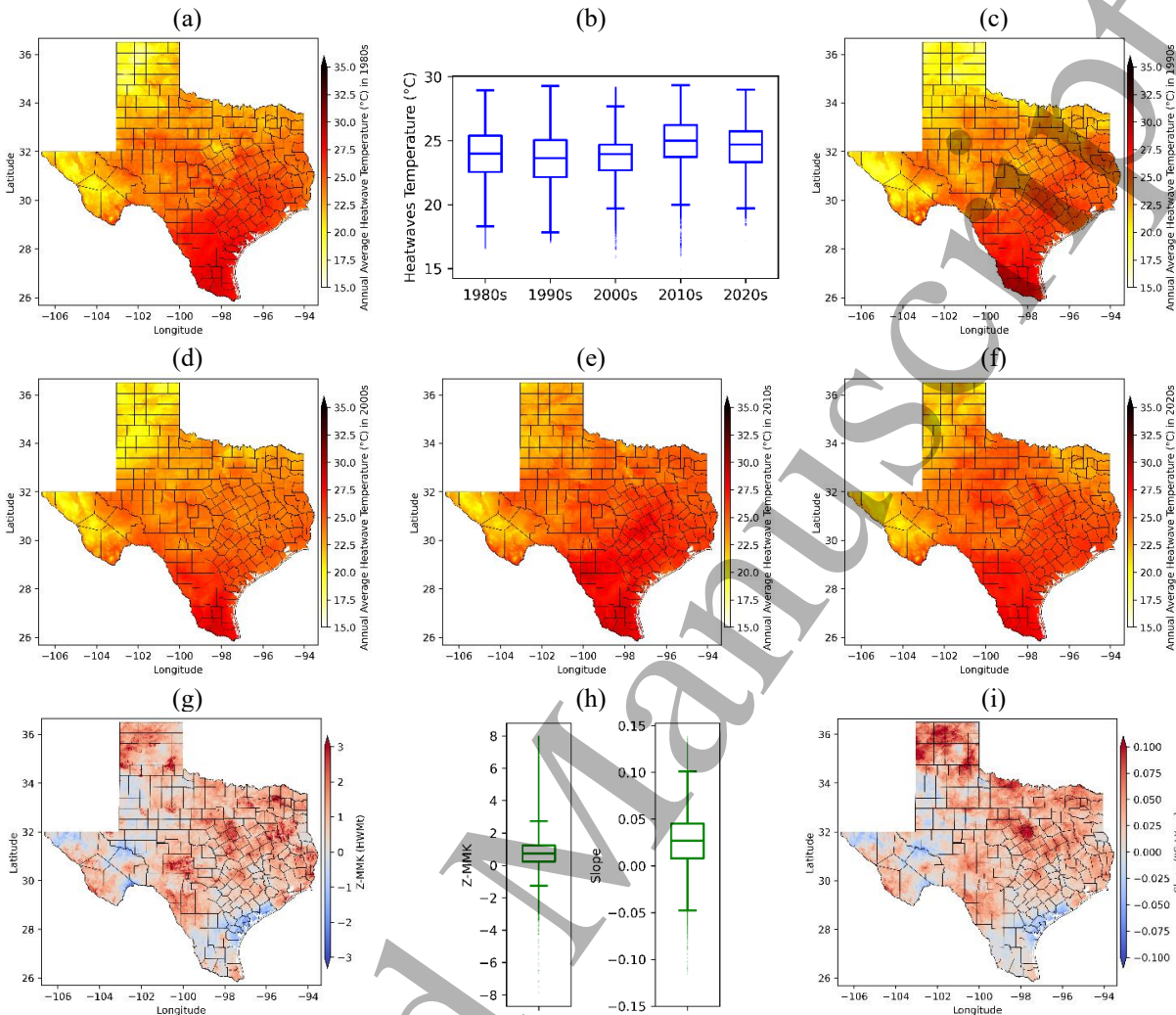


Figure 8: Spatiotemporal variability in mean temperature of heatwaves in a year (HWMt) across the 1980s, 1990s, 2000s, 2010s, and 2020s (subplots a, c, d, e, and f, respectively); statistical summary of HWMt shown as a boxplot (subplot b); Z-values from the MMK trend test (subplot g) and Sen's slope of the trend in HWMt during 1980 to 2023 (subplot i); statistical summaries of the Z-values and Sen's slope presented as boxplot (subplot h)

Unlike HWMt, HWAt has increased significantly across Texas since the 1980s, as shown in (Figure 9a, c, d, e, f). The average HWAt increased from 28.6 °C in the 1980s to 31.5 °C in the 2020s, representing an overall rise of approximately 2.9 °C (Figure 9b). In the 1980s, 55 counties recorded average HWAt values above 30 °C, with none exceeding 33 °C (Figure 9a), whereas in the 2020s, 224 counties exhibited average HWAt greater than 30 °C and 22 counties (including Ward, Webb, Dimmit, Zapata, and Maverick) exceeded 33 °C (Figure 9f). In contrast, counties such as Marion, Kerr, Real, Rusk, Dallam, Lipscomb, and Harrison recorded the lowest average HWAt in the 2020s (Figure 9f), with values below 29 °C. The highest increases were concentrated in the Panhandle and parts of west and central Texas (Figure 9a, f), where counties such as Moore, Sherman, Oldham, Potter, Hutchinson, Erath, Deaf Smith, Reeves, Hansford, Culberson, Parmer,

and Hartley exhibited increases of more than 5 °C in average HWAt between the 1980s and the 2020s. Metropolitan counties also experienced substantial increases, with Dallas rising from about 29.1 °C in the 1980s to 33.1 °C in the 2020s and Harris from 29.5 °C to 32.1 °C, with the 2010s marking particularly large jumps (Figure 9e). In contrast, humid or coastal counties, such as Rusk and Aransas, exhibited decrease of 0.2 to 0.3°C in HWAt (Figure 9f). The Z-MMK results further support the widespread increase in HWAt (Figure 9g), with 216 counties exhibiting statistically significant positive trends. The statewide average trend slope indicates a rate of increase of approximately 0.6 °C/decade (Figure 9h), with 29 counties exhibiting slopes exceeding 0.8 °C/decade. The highest rate of increase in HWAt, at 1.1 °C per decade, was observed in Somervell and Delta counties. The hotspots of higher trend slopes were primarily concentrated in the Panhandle, North Texas, and parts of West Texas (Figure 9i), corroborating the findings of the decadal HWAt analysis.

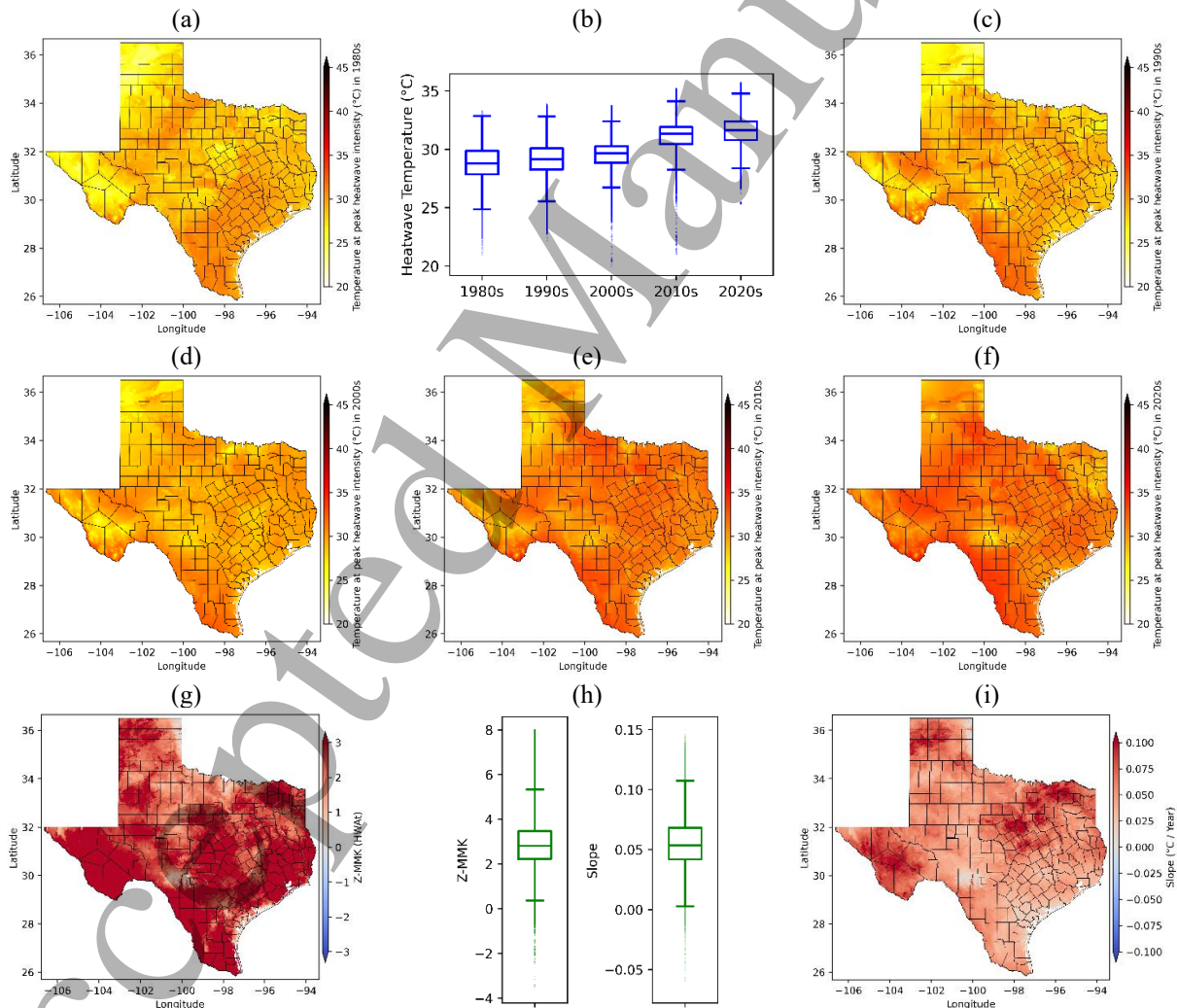


Figure 9: Spatiotemporal variability in temperature corresponding to peak heatwave intensity (HWAt) across the 1980s, 1990s, 2000s, 2010s, and 2020s (subplots a, c, d, e, and f, respectively); statistical summary of HWAt shown as a boxplot (subplot b); Z-values from the

MMK trend test (subplot g) and Sen's slope of the trend in HWT during 1980 to 2023 (subplot i); statistical summaries of the Z-values and Sen's slope presented as boxplot (subplot h)

#### 4.5 Heatwave Onset

The timing of first heatwave event of the year reveals critical information about the shifting onset of extreme heat in Texas. Spatial and temporal analyses indicate a marked evolution in HWT patterns from the 1980s through the 2020s (Figures 10a, c, d, e, f). In the 1980s, the statewide average HWT occurred on the 109th day (Figure 10b) of the year ( $\approx$  late April). Twelve counties, Bailey, Hockley, Nueces, Cooke, Matagorda, Kleberg, Calhoun, Hansford, Kenedy, Runnels, San Patricio, and Willacy, recorded HWT values exceeding the 135th day (i.e., mid-May), whereas seven counties, Franklin, Bowie, Dickens, Titus, Bastrop, Rains, and Red River, exhibited HWT values below the 75th day, i.e., mid-March (Figure 10a). The 1990s followed a similar pattern (Figure 10c), with an average HWT occurring on the 103rd day (Figure 10b). A pronounced shift occurred in the 2000s, when the statewide average HWT advanced to day 62 ( $\approx$  early March), about 1.5 months earlier than 1980s (Figure 10b, d). Approximately 75% of counties (191 counties) experienced an onset that was at least one month earlier, while 77 counties exhibited an onset that was at least two months earlier in the 2000s compared to the 1980s. Counties such as Hockley, Bailey, and Willacy even experienced an onset that was at least three months earlier. The earliest heatwave onsets were observed particularly in east and west Texas (Figure 10d). This decade represents a structural break in the seasonal timing of extreme heat in Texas. In the 2010s, the statewide mean shifted later again to 68th day ( $\approx$  mid-March), with a similar spatial pattern with 2000s (Figure 10b, e). By the 2020s, the mean HWT further shifted to the 81st day ( $\approx$  late March), while spatial variability increased substantially (Figure 10b, f). The divergence is clearly reflected in the map, with west, south, and coastal Texas experiencing extremely early heatwave onset, whereas central and northern regions exhibit later onset (Figure 10f). Notably, later onsets (HWT >120th day) were observed in 43 counties, whereas earlier onsets (HWT <60th day) occurred in 85 counties. Counties such as Hudspeth, Jeff Davis, Galveston, Cameron, Willacy, Kenedy, and Hidalgo exhibited heatwave onset before the 35th day of the year, whereas counties such as Concho, Runnels, Somervell, Coleman, Mason, Kimble, Menard, McCulloch, Nolan, Taylor, Real, and Edwards experienced onset after the 150th day. Given that major urban centers are predominantly located in the coastal region, a substantial share of the population is increasingly experiencing earlier onset of heat stress. The early onset of heatwaves is further corroborated by the Z-MMK results (Figure 10g) and the Sen's slope estimates (Figure 10i). Approximately 93% of the counties (237 counties) exhibited negative trends in HWT (Figure 10g), indicating progressively earlier heatwave onset, of which 15 counties showed statistically significant negative trends. The spatial map illustrate the dominance of negative trend across most of the state, particularly in west, east, south and coastal regions (Figure 10g). The statewide average trend slope was estimated at  $-6.2$  days per decade (Figure 10h), with 47 counties exhibiting slopes below  $-10$  days per decade (Figure 10i). Counties such as Midland, Martin, Ector, Calhoun, Dawson, Glasscock, Yoakum, Terry, Aransas, Hockley, and Bailey exhibited the steepest negative slopes,

with values below  $-15$  days/decade. In contrast, Wheeler, Hemphill, Edwards, and Lipscomb counties showed the strongest positive slopes, with values exceeding  $+5$  days per decade. From an applied perspective, the earlier onset of heatwaves compresses the cool-season window for agriculture, outdoor work, and infrastructure maintenance. The significant regional contrasts can further complicate planning, as risk management strategies that suffice for one region may not be adequate in another region.

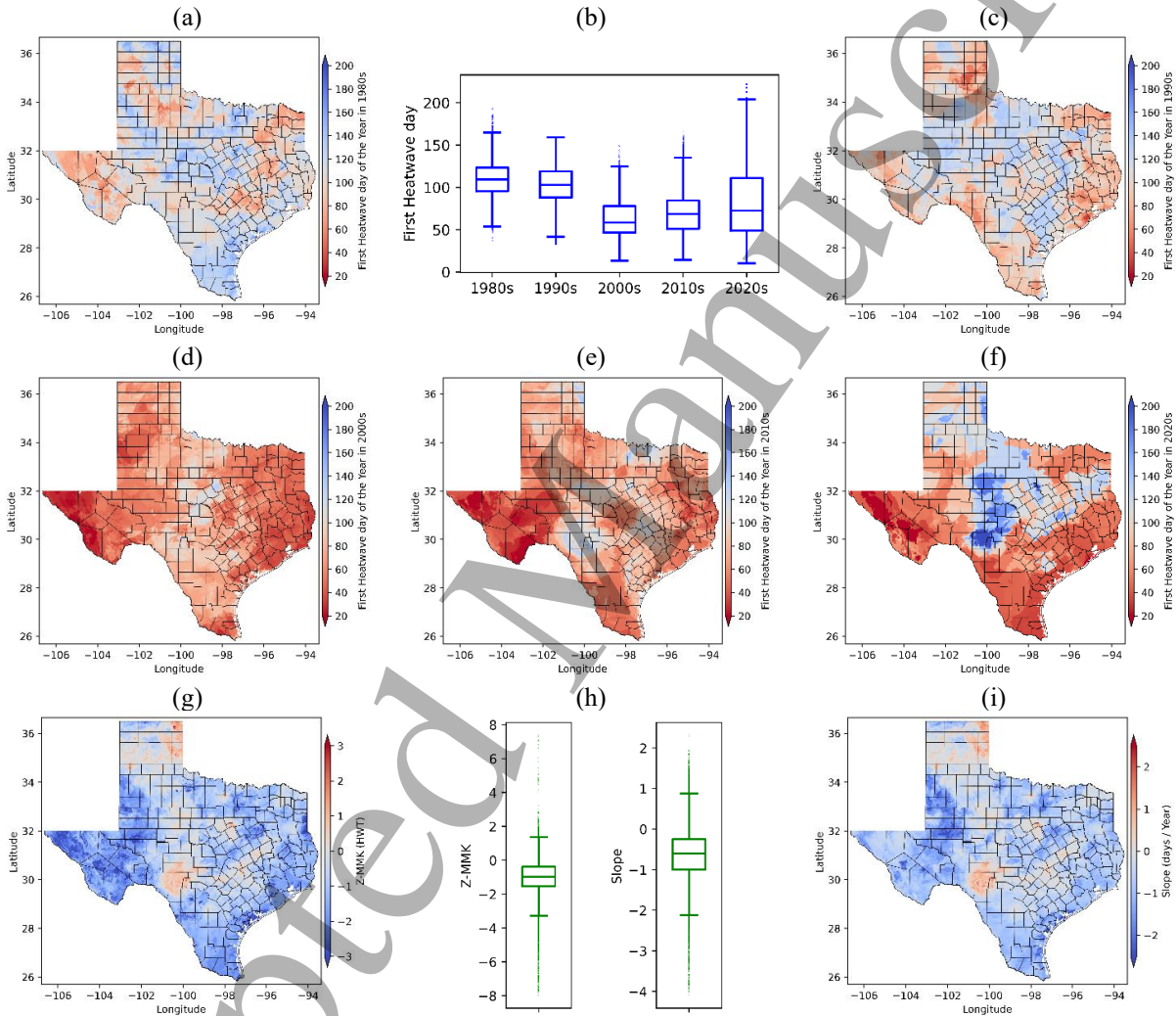


Figure 10: Spatiotemporal variability in the onset day of the first heatwave event of the year (HWT) across the 1980s, 1990s, 2000s, 2010s, and 2020s (subplots a, c, d, e, and f, respectively); statistical summary of HWT shown as a boxplot (subplot b); Z-values from the MMK trend test (subplot g) and Sen's slope of the trend in HWT during 1980 to 2023 (subplot i); statistical summaries of the Z-values and Sen's slope presented as boxplot (subplot h)

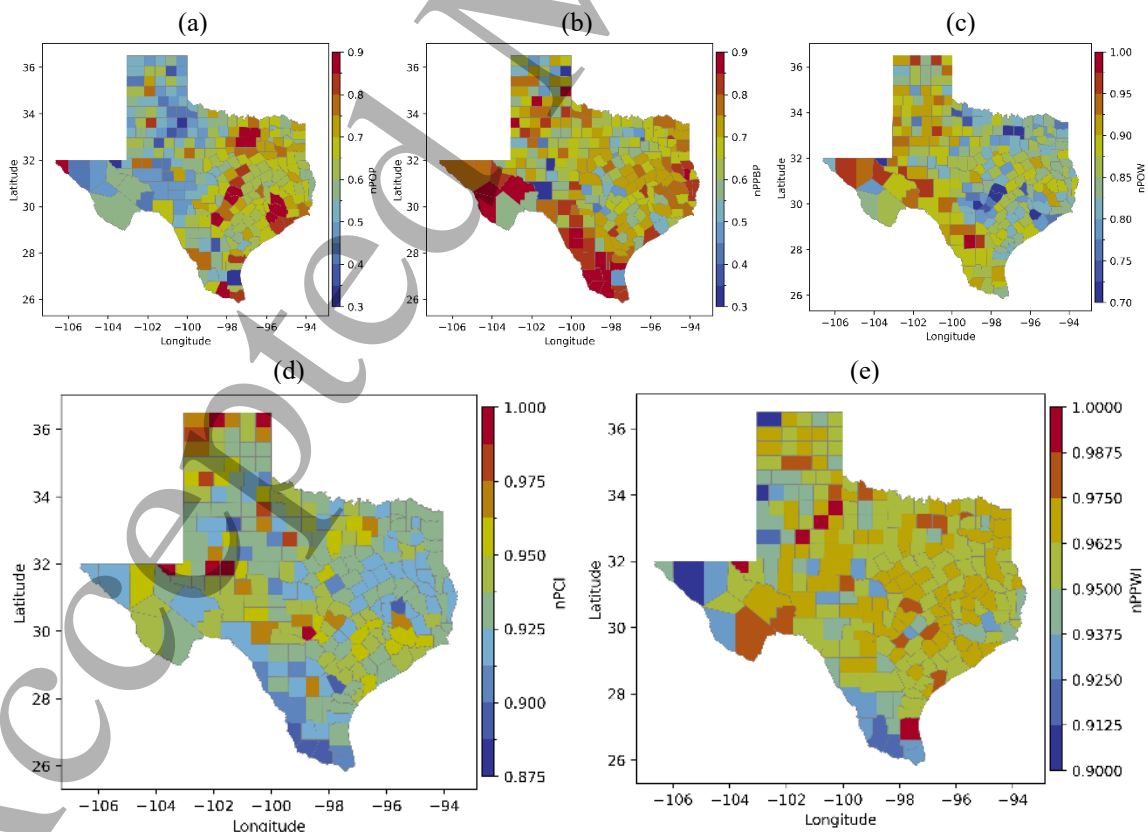
#### 4.6 Heatwave Vulnerability

Heatwaves encompass multiple dimensions, such as frequency, duration, and intensity/severity, therefore a single metric is needed to capture their combined hazard. To address this, a composite

1  
2  
3 indicator, CHI, was developed, and its spatial distribution is presented in Figure 11f. The CHI map  
4 reveals a clear spatial pattern of heatwave hazard across Texas, with substantial gradients between  
5 the western, southern, coastal, and northern parts of the state. Higher CHI values indicate greater  
6 heatwave hazard and potentially higher risk, whereas lower values correspond to lower hazard and  
7 lower risk. Among the 254 counties analyzed, 8 recorded CHI values greater than 0.8, 55 ranged  
8 from 0.6 to 0.8, 90 ranged from 0.4 to 0.6, 77 ranged from 0.2 to 0.4, and 24 exhibited values  
9 below 0.2. A prominent cluster of high CHI values is concentrated in coastal counties adjacent to  
10 the Houston metropolitan region (Figure 11f). Other hotspots of higher CHI were observed in west  
11 Texas and Lower Rio Grande valley. Counties such as Galveston, Harris, Chambers, Montgomery,  
12 Brazoria, Fort Bend, Brewster, and Liberty exhibited the highest values of CHI, indicating severe  
13 heatwave hazard in these counties. In contrast, counties such as Ochiltree, Wheeler, Hansford,  
14 Sherman, Edwards, Dallam, Hemphill, Real, and Lipscomb exhibited the lowest values of CHI,  
15 indicating very low risk of heatwave hazard. The lower CHI were mainly observed over northern  
16 Texas and some parts of central Texas. These patterns indicate that heatwaves in Texas are not  
17 spatially uniform, possibly due to interactions among regional climate regimes, atmospheric  
18 circulation patterns, land–surface characteristics, and, in some cases, urbanization effects.  
19  
20  
21  
22  
23  
24

25 The spatial distribution of CHI further informs the assessment of heatwave vulnerability (HVI). In  
26 line with the spatial gradients captured by CHI, the HVI, constructed by integrating composite  
27 heatwave hazard with demographic exposure such as elderly and children population, population  
28 below poverty and outdoor workers (Figure 11a, b, c), and socio-economic adaptive capacity such  
29 as per capita income and population with health-insurance (Figure 11d, e), shows a similarly  
30 heterogeneous distribution across Texas, closely aligning with the underlying hazard patterns. The  
31 HVI map (Figure 11g) indicates that the most vulnerable counties are primarily concentrated in  
32 the coastal region, west Texas, and the lower Rio Grande Valley, similar to CHI. Counties including  
33 Harris, Hidalgo, Galveston, Webb, Liberty, Willacy, Jefferson, Zapata, San Jacinto, Chambers,  
34 Montgomery, Ector, Pecos, Duval, Starr, Presidio, Brazoria, Cameron, El Paso, Midland, Kleberg,  
35 Caldwell, Jim Wells, Polk, Atascosa, Fort Bend, Bexar, Trinity, and Jeff Davis were identified  
36 among the 30 most vulnerable counties. In contrast, counties such as Hall, Randall, Somervell,  
37 Donley, Archer, Moore, Gray, Armstrong, Briscoe, Kimble, Grayson, Cooke, Bandera, Lamb,  
38 Oldham, Roberts, Montague, Collingsworth, Clay, Kerr, Ochiltree, Hartley, Wheeler, Hansford,  
39 Sherman, Edwards, Dallam, Hemphill, Real, and Lipscomb emerged as 30 least vulnerable  
40 counties. The spatial maps also indicates that although many areas experience notable heatwave  
41 hazard, only a subset of counties combine that hazard with high exposure and weaker adaptive  
42 capacity to produce truly critical levels of vulnerability. For example, of the 30 counties  
43 experiencing the most severe heatwave hazard, only 23 are among the 30 most vulnerable counties,  
44 indicating that elevated hazard alone does not necessarily translate into higher vulnerability, due  
45 to less population exposure or higher adaptive capacity or combination of both. Conversely, only  
46 23 of the 30 most vulnerable counties overlapped with the 30 counties having the highest CHI.  
47  
48  
49  
50  
51  
52  
53  
54  
55  
56  
57  
58  
59  
60

1  
2  
3 higher exposure or lower adaptive capacity, despite not being in the top 30 counties with the  
4 highest CHI values. In coastal counties, close to Houston metropolitan region, higher CHI coincide  
5 with large exposed population, resulting higher vulnerability, despite having relatively high per-  
6 capita income in parts of this corridor. Similarly, higher HVI values in the lower Rio Grande valley  
7 (e.g., Hidalgo, Cameron, and Webb counties) reflect the convergence of higher CHI with higher  
8 exposure and comparatively lower adaptive capacity, highlighting these border counties as another  
9 critical zone for heat-health risk. Other notable pockets of high vulnerability emerge in and around  
10 major inland urban centers including Bexar, El Paso, Midland and Ector show higher HVI values,  
11 driven by a combination of higher CHI, moderate to large exposure, and lower adaptive capacity.  
12 The results also suggest that climatic effects, outdoor labor, and unequal access to cooling and  
13 healthcare may amplify heat impacts in large cities and industrial regions, even where average  
14 income is not the lowest in the state. In contrast, many counties in the Panhandle region and parts  
15 of north and central Texas exhibit lower vulnerability, where both heatwave hazard and population  
16 exposure are relatively low, and adaptive capacity is not strongly disadvantageous. In these  
17 sparsely populated regions, even when heatwaves occur, the number of people exposed is small  
18 and basic socio-economic conditions are generally sufficient to limit widespread vulnerability. The  
19 HVI therefore provides a policy-relevant perspective than hazard alone, pinpointing where  
20 heatwave preparedness, targeted outreach to sensitive groups, improvements in housing quality  
21 and access to cooling, and strengthening of public health infrastructure are most urgently needed  
22 across Texas.



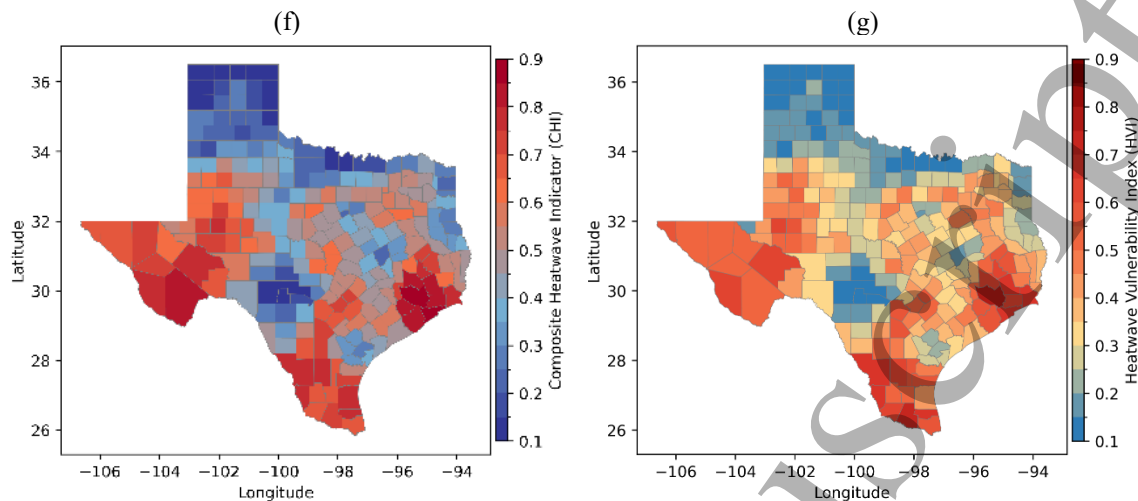


Figure 11: Spatial variability of (a) normalized vulnerable population (nPOP), (b) normalized percentage population below poverty (nPPBP), (c) normalized percentage of outdoor workers (nPOW), (d) normalized per capita income (nPCI), (e) normalized percentage population with health-insurance (nPPWI), (f) composite heatwave indicator (CHI), and (g) Heatwave Vulnerability Index (HVI)

## 5 Discussion

The spatiotemporal patterns of heatwave characteristics identified in this study provide compelling evidence that Texas has undergone a substantial and multidimensional intensification of extreme heat over the last four decades. The concurrent rise in frequency, duration, amplitude, and earlier onset of heatwaves aligns with broader warming trends documented at regional and national scales (Smith et al., 2013; Habeeb et al., 2015), yet the magnitude and spatial heterogeneity revealed here underscore that Texas is emerging as a key hotspot of accelerating extreme heat. These findings are consistent with previous assessments that show disproportionate warming of hot extremes in the southern United States, driven by both thermodynamic warming and land-atmosphere feedbacks that amplify persistent heat (Vose et al., 2017; Miralles et al., 2019). The rapid escalation in HWN and HWF since the 2000s mirrors earlier studies noting the increased persistence of precipitation deficit, higher evapotranspiration, and soil-moisture depletion as dominant processes intensifying heatwaves in Texas (Nielsen-Gammon, 2012; Rupp et al., 2015). The marked increase in heatwave frequency corroborates findings from Rupp et al. (2012 and 2015), who showed that anthropogenic warming substantially increased the likelihood of extreme heat in Texas during events such as summer 2011. Likewise, Habeeb et al. (2015) found that major U.S. cities, including Dallas, and Fort Worth in Texas, have experienced significant increases in heatwave frequency, consistent with the strong county-level increases in HWF observed here. The amplification of summer heat frequency in Texas has also been linked to the enhanced Pacific zonal Sea Surface Temperature (SST) gradient, which supports persistent ridge formation over the south-central U.S. (Deng et al., 2018). Our results, which show some counties gaining more than 10 additional heatwave days per decade, reinforce the growing evidence that Texas lies at the confluence of

1  
2  
3 large-scale ocean–atmosphere anomalies and regional land–surface feedbacks that favor extreme  
4 and persistent heat. The systematic increase in heatwave duration suggests that heatwaves in Texas  
5 are becoming not only more frequent but also more persistent. The average HWD tripling from  
6 6.3 to 16.3 days echoes the prolonged heat events observed in major historical years such as 1998  
7 and 2011, during which precipitation deficit produced prolonged subsidence and clear-sky  
8 radiation excess (Nielsen-Gammon, 2012). The presence of county-level slopes exceeding 2.5  
9 days per decade, particularly in western and central Texas, signals a transition toward a climate  
10 regime where multi-week heatwaves may become common in the mid-21st century, with  
11 substantial implications for agriculture, outdoor labor, reservoir evaporation, and electricity  
12 demand. Meehl and Tebaldi (2004) demonstrated that the atmospheric circulation pattern  
13 associated with current heatwaves in Europe and North America is amplified by rising greenhouse-  
14 gas concentrations, implying a future increase in the severity of such events.  
15  
16  
17  
18  
19

20 The increase in HWA since the 1980s and the widespread significant trends in HWA<sub>t</sub> confirm that  
21 the upper bound of extreme heat in Texas is rising rapidly. This result is consistent with projections  
22 that hot extremes increase more sharply than mean temperatures due to nonlinear processes such  
23 as vapor-pressure-deficit amplification, soil desiccation, and boundary-layer deepening during  
24 drought (Perkins-Kirkpatrick & Lewis, 2020). The spatial expansion of high-intensity peaks into  
25 historically cooler areas of north Texas and the Panhandle is particularly noteworthy. While these  
26 regions once had strong nocturnal radiative cooling and relatively mild summer maxima, recent  
27 studies have shown decreasing soil moisture and increasing aridity in high plains ecosystems,  
28 leading to escalating daytime heat extremes (Rupp et al., 2017).  
29  
30  
31

32 The observed shift toward earlier heatwave onset, indicates that the heat season in Texas is  
33 expanding, consistent with national assessments showing earlier warm-season thresholds across  
34 much of the southern U.S. (EPA, 2022). Early onset is particularly consequential for agriculture,  
35 where crop planting schedules and early-season vegetation are sensitive to late-spring heat surges.  
36 Earlier heatwaves also reduce the physiological acclimatization window for populations,  
37 increasing early-season heat-related health risks (Perkins & Alexander, 2013). The strong negative  
38 trends in west, south, and coastal Texas align with regions that already experience early warm-  
39 season onset due to proximity to the subtropical ridge.  
40  
41  
42  
43

44 The CHI developed in this study reveals three major hazard clusters, Houston metropolitan region,  
45 west Texas, and the lower Rio Grande valley. The Houston region exhibits strong urban heat-island  
46 amplification, high humidity, and a growing population base, factors shown to intensify heat stress  
47 exposure in past studies (Habeeb et al., 2015). West Texas represents an arid-climate hotspot where  
48 soil-moisture feedbacks and drought intensification enhance heatwave persistence (Rupp et al.,  
49 2015). The lower Rio Grande valley is characterized by high baseline temperatures, population  
50 growth, and humidity, which together create climatic conditions conducive to intense heat stress.  
51 The overlap of these independent mechanisms explains the consistent CHI clustering observed in  
52 this study. The vulnerability patterns identified using HVI highlight that hazard severity alone does  
53 not fully explain risk. Many high-hazard counties, especially in parts of west Texas, exhibit  
54  
55  
56  
57  
58  
59  
60

1  
2  
3 moderate or low vulnerability due to low population and moderate-income levels. Conversely,  
4 several urban counties (e.g., Dallas, Tarrant, Bexar, Harris) show elevated vulnerability despite  
5 moderate CHI because of large exposed populations and socioeconomic disparities. This  
6 asymmetry confirms the broader conclusion from heat-health literature that vulnerability is co-  
7 determined by demographic sensitivity and inequitable adaptive capacity (Wolf & McGregor, 2013;  
8 Williams et al., 2012). The lower Rio Grande valley stands out as a region where high CHI  
9 converges with high exposure and lower-income communities, reinforcing the findings that border  
10 counties experience disproportionately elevated heat-health risks. Similarly, the high vulnerability  
11 observed in coastal counties, even those with higher incomes, likely reflects combined hazards of  
12 humidity-driven heat stress, urbanization, industrial activity, and high population density. The  
13 spatial differentiation between CHI and HVI underscores the value of moving beyond purely  
14 meteorological assessments toward integrated climate–societal risk frameworks.  
15  
16  
17  
18  
19

20 The results from this study carry significant implications for heat-risk governance. As heatwaves  
21 become longer, more frequent, and earlier, Texas’s infrastructure systems, electricity, water supply,  
22 public health, and agriculture, face growing simultaneous pressures. Past events, such as the 2011  
23 heatwave and corresponding electricity emergency declarations, demonstrate that extreme heat can  
24 push the power grids to near-failure (Combs, 2012). Earlier and more severe heatwaves will  
25 increase cooling demand months earlier than historically expected, requiring grid planning that  
26 explicitly considers climatological shifts. In agricultural regions, longer heatwaves may compound  
27 drought impacts, reduce yields, and stress livestock, as documented in previous analyses of heat  
28 and soil moisture interactions (Lobell et al., 2011). Urban areas may require expanded cooling  
29 centers, targeted outreach to vulnerable groups, and urban greening interventions to mitigate  
30 intensifying heat-island effects. Furthermore, the strong county-level heterogeneity in  
31 vulnerability suggests that adaptation strategies must be region-specific. Border counties may  
32 require integrated health-centric strategies, while west Texas may prioritize drought and heat-  
33 resilient agricultural systems. Coastal regions, facing both high heat and humidity, will require  
34 interventions that integrate humidity-adjusted heat metrics and resilience to compounding hazards.  
35  
36  
37  
38  
39

40 Despite the robustness of heatwave characteristics identified in this study, several limitations  
41 should be acknowledged. First, the analysis relies on gridded temperature data from the Daymet  
42 dataset, which, although high-resolution (~1 km), is subject to uncertainties arising from  
43 interpolation methods and station density. Validation against in situ station observations indicates  
44 that Daymet temperature (minimum and maximum) exhibits the strongest correlation and lowest  
45 error among the evaluated datasets, outperforming alternatives such as GridMET and PRISM,  
46 however, its performance and relative superiority vary across different climatic zones (Essou et al.,  
47 2016; Bandaru et al., 2017; Spangler et al., 2019; Ahn et al., 2024). Nevertheless, despite this  
48 comparatively superior performance, inherent uncertainties persist due to interpolation techniques  
49 and spatial representation. Specifically, heatwave characteristics derived from Daymet tend to be  
50 underpredicted relative to station observations, likely due to smoothing effects in gridded data  
51 (Ahn et al., 2024). Conversely, the high spatial resolution of Daymet can lead to overestimation of  
52  
53  
54  
55  
56  
57  
58  
59  
60

1  
2  
3 heatwave occurrence compared to coarser-resolution datasets, as it captures localized extremes  
4 that are often averaged out at broader scales. These contrasting behaviors underscore a key  
5 limitation in heatwave analysis, namely the sensitivity of results to dataset choice and spatial  
6 resolution. Therefore, while Daymet provides a reliable basis for regional analysis, caution is  
7 warranted when interpreting absolute magnitudes of heatwave metrics, and future work should  
8 emphasize multi-dataset comparisons and station-based validation.  
9

10  
11 Moreover, the vulnerability assessment, remains constrained by the selection of socioeconomic  
12 indicators. Although, the vulnerability assessment in this study incorporates socio-economic  
13 indicators such as population under 5 years and above 65 years, per capita income, percentage of  
14 population below poverty, percentage of outdoor workers, and percentage of population with  
15 health insurance to better represent exposure and adaptive capacity, this remains a limitation. Heat  
16 vulnerability is inherently multidimensional, and important factors such as housing quality, access  
17 to cooling infrastructure, urban green space, pre-existing health conditions, and other potentially  
18 important factors were not included due to data limitations. The exclusion of such variables may  
19 therefore lead to an incomplete characterization of vulnerability patterns. Hence, future studies  
20 should aim to incorporate a broader and more dynamic set of indicators to better capture the  
21 complexity of heat-related risk.  
22  
23  
24  
25  
26

27 In addition to indicator selection, the temporal aggregation of heatwave characteristics may also  
28 influence vulnerability interpretation. Annual aggregation was used in this study to assess  
29 heatwaves as an evolving year-round climate signal rather than as a fixed summer-season  
30 phenomenon. This approach helps capture broader changes in heatwave timing, duration,  
31 cumulative exposure, and long-term trends across the full calendar year, including the expansion  
32 of heat stress into earlier or later parts of the year. From a policy perspective, annual aggregation  
33 can support calendar-wide heat-risk management by highlighting that preparedness and adaptation  
34 planning may need to extend beyond the traditional summer season. However, this approach may  
35 also mask season-specific trends in heatwave characteristics, particularly during peak summer  
36 when heatwaves are often most severe. For example, annual trends may reflect increasing  
37 heatwave occurrence in early or late seasons, while summer-specific trends may differ in  
38 magnitude, spatial extent, or even direction. Therefore, the vulnerability estimates derived from  
39 annual heatwave characteristics should be interpreted as indicators of cumulative year-round  
40 exposure rather than summer-specific heat risk. Future studies should incorporate seasonally  
41 resolved heatwave analyses to better distinguish between peak-summer intensification and  
42 seasonal expansion of heatwave conditions, thereby supporting more targeted vulnerability  
43 interpretation and season-specific adaptation strategies.  
44  
45  
46  
47  
48  
49

## 50 **6 Summary and Conclusion**

51  
52 This study provides a comprehensive spatiotemporal evaluation of heatwave characteristics across  
53 Texas over the period 1980–2023, employing Daymet high-resolution temperature data and a suite  
54 of excess heatwave indicators. Using the EHF framework, multiple metrics, including HWN, HWF,  
55 HWD, HWL, HWA, HWM, HWAt, HWMt, and HWT, were analyzed to characterize key  
56  
57  
58  
59  
60

1  
2  
3 dimensions of heatwaves such as frequency, duration, intensity, and onset timing. In addition, a  
4 composite heatwave hazard index (CHI) was developed by integrating these indicators to provide  
5 a holistic representation of heatwave severity. This hazard component was further combined with  
6 demographic exposure and adaptive capacity to assess heatwave vulnerability across Texas. The  
7 main findings from this study are summarized below:  
8  
9

- 10 (i) Heatwave frequency has raised significantly, with statewide average HWN increasing  
11 from ~3.6 events in the 1980s to ~9 events in the 2020s, a 147% increase, and 97% of  
12 counties showing statistically significant positive trends. The HWF has also increased  
13 from ~16 days in 1980s to ~63 days in 2020s.
- 14 (ii) The duration of heatwave has lengthened, with statewide average HWL increased from  
15 ~4.5 days in 1980s to ~6.8 days in 2020s, while the HWD increased from 6.3 to 16.3  
16 days.
- 17 (iii) Peak intensity of heatwave (HWA) increased from ~20 °C<sup>2</sup> in the 1980s to ~37 °C<sup>2</sup> in  
18 the 2020s, an 83% rise, with 170 counties showing statistically significant trends.
- 19 (iv) Peak heatwave temperature (HWAt) increased by ~2.9 °C, with 216 counties exhibiting  
20 statistically significant trend.
- 21 (v) Heatwave onset shifted earlier by an average of 6.2 days/decade, with 237 counties  
22 showing statistically significant negative trends. In some extreme cases, onsets have  
23 shifted 2–3 months earlier.
- 24 (vi) The highest composite heatwave hazard was concentrated in three major clusters across  
25 Texas, with one cluster covering the Houston metropolitan area including Galveston,  
26 Harris, Chambers, Montgomery, and nearby counties, another cluster spanning West  
27 Texas including Brewster, Presidio, and adjacent counties, and a third cluster located  
28 in the Lower Rio Grande Valley including Willacy, Webb, Zapata, and surrounding  
29 counties.
- 30 (vii) Maximum vulnerability was observed in Harris, Galveston, and Jefferson counties in  
31 the Houston area, El Paso, Presidio, and Midland counties in west Texas, and Hidalgo,  
32 and Webb counties in the Lower Rio Grande Valley.

33  
34  
35  
36  
37  
38  
39  
40  
41  
42 The findings of this study reveal that heatwaves in Texas have shifted from relatively infrequent  
43 extremes in the late twentieth century to recurrent and increasingly severe hazards in the first  
44 quarter of the twenty-first century. The simultaneous rise in heatwave frequency, duration, and  
45 intensity carries significant implications for public health, agricultural productivity, energy  
46 demand, and water resources. These results underscore the urgent need for targeted adaptation  
47 measures, including early warning systems, occupational heat-safety protocols, urban heat-  
48 mitigation strategies, climate-resilient agricultural practices, and integrated water–energy  
49 management. Future work should expand this framework by incorporating climate projections,  
50 sector-specific vulnerability assessments, and impact-based modeling.  
51  
52  
53  
54  
55  
56  
57  
58  
59  
60

### Author Contributions

Deen Dayal: conceptualization, methodology, data curation, formal analysis, investigation, visualization, writing – original draft. Santosh S. Palmate: conceptualization, investigation, writing – review and editing. Rosario Sanchez: investigation, writing – review and editing.

### Acknowledgements

The authors would like to sincerely acknowledge the Texas A&M AgriLife Research Center at El Paso, Texas A&M University System, for providing the necessary support and facilities to conduct this research work.

### Funding

This project is based on research that was partially supported by the Texas A&M AgriLife Research Center at El Paso with funding from the Hatch Act capacity funding program Accession Numbers 7006746 (S1089 old) and 7010850 (S1089 new) from the U.S. Department of Agriculture (USDA), National Institute of Food and Agriculture (NIFA).

### Conflicts of Interest

The authors declare no competing financial or non-financial interests.

### Data Availability Statement

The climate data used in this study were obtained from the Daymet dataset, which provides daily gridded meteorological variables and is publicly available through the Oak Ridge National Laboratory Distributed Active Archive Center (ORNL DAAC; <https://daymet.ornl.gov/>).

### References

- Allen, C. D., Macalady, A. K., Chenchouni, H., Bachelet, D., McDowell, N., Vennetier, M., ... & Cobb, N. (2010). A global overview of drought and heat-induced tree mortality reveals emerging climate change risks for forests. *Forest ecology and management*, 259(4), 660-684.
- Angélil, O., Stone, D., Wehner, M., Paciorek, C. J., Krishnan, H., & Collins, W. (2017). An independent assessment of anthropogenic attribution statements for recent extreme temperature and rainfall events. *Journal of Climate*, 30(1), 5-16.
- Ahn, Y., Tuholske, C., & Parks, R. M. (2024). Comparing approximated heat stress measures across the United States. *GeoHealth*, 8(1), e2023GH000923.
- Argüeso, D. (2024). dargueso/EHF: v2.2 (v2.2). Zenodo. <https://doi.org/10.5281/zenodo.13622471>

- 1  
2  
3 Bandaru, V., Pei, Y., Hart, Q., & Jenkins, B. M. (2017). Impact of biases in gridded weather datasets  
4 on biomass estimates of short rotation woody cropping systems. *Agricultural and Forest*  
5 *Meteorology*, 233, 71-79.  
6  
7  
8 Barriopedro, D., Fischer, E. M., Luterbacher, J., Trigo, R. M., & García-Herrera, R. (2011). The  
9 hot summer of 2010: redrawing the temperature record map of Europe. *Science*, 332(6026),  
10 220-224.  
11  
12 Chegini, T., Li, H. Y., & Leung, L. R. (2021). HyRiver: Hydroclimate data retriever. *Journal of*  
13 *Open Source Software*, 6(66), 3175.  
14  
15  
16 Combs, S. (2012). The impact of the 2011 drought and beyond. *Texas Comptroller of Public*  
17 *Accounts Special Rep., Publ*, 96(1704), 16.  
18  
19 Deng, K., Ting, M., Yang, S., & Tan, Y. (2018). Increased frequency of summer extreme heat waves  
20 over Texas area tied to the amplification of Pacific zonal SST gradient. *Journal of*  
21 *Climate*, 31(14), 5629-5647.  
22  
23  
24 EPA, U. (2022). Climate change indicators: Heat waves. *Environment Protection Agency*.  
25  
26 Essou, G. R., Arsenault, R., & Brissette, F. P. (2016). Comparison of climate datasets for lumped  
27 hydrological modeling over the continental United States. *Journal of Hydrology*, 537, 334-345.  
28  
29 Fischer, E. M., Seneviratne, S. I., Lüthi, D., & Schär, C. (2007). Contribution of land-atmosphere  
30 coupling to recent European summer heat waves. *Geophysical Research Letters*, 34(6).  
31  
32 Gasparrini, A., Guo, Y., Hashizume, M., Lavigne, E., Zanobetti, A., Schwartz, J., ... & Armstrong,  
33 B. (2015). Mortality risk attributable to high and low ambient temperature: a multicountry  
34 observational study. *The lancet*, 386(9991), 369-375.  
35  
36  
37 Habeeb, D., Vargo, J., & Stone Jr, B. (2015). Rising heat wave trends in large US cities. *Natural*  
38 *Hazards*, 76(3), 1651-1665.  
39  
40  
41 Hamed, K. H., & Rao, A. R. (1998). A modified Mann-Kendall trend test for autocorrelated  
42 data. *Journal of hydrology*, 204(1-4), 182-196.  
43  
44 Hatvani-Kovacs, G., Belusko, M., Pockett, J., & Boland, J. (2016). Can the excess heat factor  
45 indicate heatwave-related morbidity? A case study in Adelaide, South  
46 Australia. *EcoHealth*, 13(1), 100-110.  
47  
48 Hussain, M., & Mahmud, I. (2019). pyMannKendall: a python package for non parametric Mann  
49 Kendall family of trend tests. *Journal of open source software*, 4(39), 1556.  
50  
51  
52 IPCC (2021). *Climate Change 2021: The Physical Science Basis*. Contribution of Working Group  
53 I to the Sixth Assessment Report of the Intergovernmental Panel on Climate Change.  
54 Cambridge University Press.  
55  
56  
57  
58  
59  
60

- 1  
2  
3 Lobell, D. B., Schlenker, W., & Costa-Roberts, J. (2011). Climate trends and global crop  
4 production since 1980. *Science*, 333(6042), 616-620.  
5  
6 McGregor, G. (2024). Heatwaves as Extreme Events. In *Heatwaves: Causes, Consequences and*  
7 *Responses* (pp. 81-133). Cham: Springer International Publishing.  
8  
9 Meehl, G. A., & Tebaldi, C. (2004). More intense, more frequent, and longer lasting heat waves in  
10 the 21st century. *Science*, 305(5686), 994-997.  
11  
12 Miralles, D. G., Gentine, P., Seneviratne, S. I., & Teuling, A. J. (2019). Land–atmospheric  
13 feedbacks during droughts and heatwaves: state of the science and current challenges. *Annals*  
14 *of the New York Academy of Sciences*, 1436(1), 19-35.  
15  
16 Mitchell, D., Heaviside, C., Vardoulakis, S., Huntingford, C., Masato, G., Guillod, B. P., ... & Allen,  
17 M. (2016). Attributing human mortality during extreme heat waves to anthropogenic climate  
18 change. *Environmental Research Letters*, 11(7), 074006.  
19  
20 Mora, C., Dousset, B., Caldwell, I. R., Powell, F. E., Geronimo, R. C., Bielecki, C. R., ... &  
21 Trauernicht, C. (2017). Global risk of deadly heat. *Nature climate change*, 7(7), 501-506.  
22  
23 Nairn, J. R., & Fawcett, R. G. (2013). *Defining heatwaves: heatwave defined as a heat-impact*  
24 *event servicing all community and business sectors in Australia*. Centre for Australian Weather  
25 and Climate Research.  
26  
27 Nairn, J., Fawcett, R., & Ray, D. (2009). Defining and predicting excessive heat events, a national  
28 system. In *Understanding High Impact Weather, CAWCR Modelling Workshop* (Vol. 30).  
29 Melbourne, Australia: Bureau of Meteorology.  
30  
31 Nairn, J., Ostendorf, B., & Bi, P. (2018). Performance of excess heat factor severity as a global  
32 heatwave health impact index. *International journal of environmental research and public*  
33 *health*, 15(11), 2494.  
34  
35 Nielsen-Gammon, J. W. (2012). The 2011 texas drought. *Texas Water Journal*, 3(1), 59-95.  
36  
37 Oliveira, A., Lopes, A., & Soares, A. (2022). Excess heat factor climatology, trends, and exposure  
38 across European functional urban areas. *Weather and Climate Extremes*, 36, 100455.  
39  
40 Perkins, S. E. (2015). A review on the scientific understanding of heatwaves—Their measurement,  
41 driving mechanisms, and changes at the global scale. *Atmospheric Research*, 164, 242-267.  
42  
43 Perkins, S. E., & Alexander, L. V. (2013). On the measurement of heat waves. *Journal of*  
44 *climate*, 26(13), 4500-4517.  
45  
46 Perkins-Kirkpatrick, S. E., & Lewis, S. C. (2020). Increasing trends in regional heatwaves. *Nature*  
47 *communications*, 11(1), 3357.  
48  
49  
50  
51  
52  
53  
54  
55  
56  
57  
58  
59  
60

- Peterson, T. C., Stott, P. A., & Herring, S. (2012). Explaining extreme events of 2011 from a climate perspective. *Bulletin of the American Meteorological Society*, 93(7), 1041-1067.
- Philip, S. Y., Kew, S. F., Van Oldenborgh, G. J., Anslow, F. S., Seneviratne, S. I., Vautard, R., ... & Otto, F. E. (2022). Rapid attribution analysis of the extraordinary heat wave on the Pacific coast of the US and Canada in June 2021. *Earth System Dynamics*, 13(4), 1689-1713.
- Robine, J. M., Cheung, S. L. K., Le Roy, S., Van Oyen, H., Griffiths, C., Michel, J. P., & Herrmann, F. R. (2008). Death toll exceeded 70,000 in Europe during the summer of 2003. *Comptes Rendus. Biologies*, 331(2), 171-178.
- Rupp, D. E., Li, S., Massey, N., Sparrow, S. N., Mote, P. W., & Allen, M. (2015). Anthropogenic influence on the changing likelihood of an exceptionally warm summer in Texas, 2011. *Geophysical Research Letters*, 42(7), 2392-2400.
- Rupp, D. E., Li, S., Mote, P. W., Massey, N., Sparrow, S. N., & Wallom, D. C. (2017). Influence of the ocean and greenhouse gases on severe drought likelihood in the central United States in 2012. *Journal of Climate*, 30(5), 1789-1806.
- Rupp, D. E., Mote, P. W., Massey, N., Rye, C. J., Jones, R., & Allen, M. R. (2012). Did human influence on climate make the 2011 Texas drought more probable. *Bull. Am. Meteorol. Soc*, 93, 1052-1054.
- Russo, S., Sillmann, J., & Fischer, E. M. (2015). Top ten European heatwaves since 1950 and their occurrence in the coming decades. *Environmental Research Letters*, 10(12), 124003.
- Sen, P. K. (1968). Estimates of the regression coefficient based on Kendall's tau. *Journal of the American statistical association*, 63(324), 1379-1389.
- Seneviratne, S. I., Zhang, X., Adnan, M., et al. (2021). *Weather and climate extreme events in a changing climate*. In: Climate Change 2021: The Physical Science Basis. IPCC AR6, Chapter 11.
- Smith, T. T., Zaitchik, B. F., & Gohlke, J. M. (2013). Heat waves in the United States: definitions, patterns and trends. *Climatic change*, 118(3), 811-825.
- Spangler, K. R., Weinberger, K. R., & Wellenius, G. A. (2019). Suitability of gridded climate datasets for use in environmental epidemiology. *Journal of exposure science & environmental epidemiology*, 29(6), 777-789.
- Teskey, R., Wertin, T., Bauweraerts, I., Ameye, M., McGuire, M. A., & Steppe, K. (2015). Responses of tree species to heat waves and extreme heat events. *Plant, cell & environment*, 38(9), 1699-1712.
- Thornton, M. M., Shrestha, R., Wei, Y., Thornton, P. E., & Kao, S.-C. (2022). *Daymet: Daily Surface Weather Data on a 1-km Grid for North America, Version 4 R1* (Version 4.1). ORNL

Distributed Active Archive Center. <https://doi.org/10.3334/ORNLDAAAC/2129> Date Accessed: 2025-05-18

- Tomlinson, C. J., Chapman, L., Thornes, J. E., & Baker, C. J. (2011). Including the urban heat island in spatial heat health risk assessment strategies: a case study for Birmingham, UK. *International journal of health geographics*, 10(1), 42.
- U.S. Census Bureau. (2023). SEX BY AGE (9 AGE CATEGORIES). *Decennial Census, DEC Detailed Demographic and Housing Characteristics File A, Table T02002*. Retrieved November 11, 2025, from [https://data.census.gov/table/DECENNIALDDHCA2020.T02002?g=040XX00US48\\$0500000&y=2020&d=DEC+Detailed+Demographic+and+Housing+Characteristics+File+A](https://data.census.gov/table/DECENNIALDDHCA2020.T02002?g=040XX00US48$0500000&y=2020&d=DEC+Detailed+Demographic+and+Housing+Characteristics+File+A).
- U.S. Census Bureau, U.S. Department of Commerce. (2024a). Income in the Past 12 Months (in 2023 Inflation-Adjusted Dollars). *American Community Survey, ACS 1-Year Estimates Subject Tables, Table S1901*. Retrieved March 30, 2026, from [https://data.census.gov/table/ACSST1Y2023.S1901?q=S1901:+Income+in+the+Past+12+Months+\(in+2023+Inflation-Adjusted+Dollars\)](https://data.census.gov/table/ACSST1Y2023.S1901?q=S1901:+Income+in+the+Past+12+Months+(in+2023+Inflation-Adjusted+Dollars)).
- U.S. Census Bureau, U.S. Department of Commerce. (2024b). Poverty Status in the Past 12 Months. *American Community Survey, ACS 5-Year Estimates Subject Tables, Table S1701*. Retrieved March 30, 2026, from [https://data.census.gov/table/ACSST5Y2023.S1701?t=Official+Poverty+Measure&g=040XX00US48,48\\$0500000&moe=false](https://data.census.gov/table/ACSST5Y2023.S1701?t=Official+Poverty+Measure&g=040XX00US48,48$0500000&moe=false).
- U.S. Census Bureau, U.S. Department of Commerce. (2024c). Sex by Occupation for the Civilian Employed Population 16 Years and Over. *American Community Survey, ACS 5-Year Estimates Detailed Tables, Table C24010*. Retrieved March 30, 2026, from [https://data.census.gov/table/ACSST5Y2023.C24010?q=C24010:+Sex+by+Occupation+for+the+Civilian+Employed+Population+16+Years+and+Over&g=040XX00US48,48\\$0500000&moe=false](https://data.census.gov/table/ACSST5Y2023.C24010?q=C24010:+Sex+by+Occupation+for+the+Civilian+Employed+Population+16+Years+and+Over&g=040XX00US48,48$0500000&moe=false).
- U.S. Census Bureau, U.S. Department of Commerce. (2024d). Health Insurance Coverage Status by Sex by Age. *American Community Survey, ACS 5-Year Estimates Detailed Tables, Table B27001*. Retrieved March 30, 2026, from [https://data.census.gov/table/ACSST5Y2023.B27001?t=Health+Insurance&g=040XX00US48,48\\$0500000&moe=false](https://data.census.gov/table/ACSST5Y2023.B27001?t=Health+Insurance&g=040XX00US48,48$0500000&moe=false).
- Vose, R. S., Easterling, D. R., Kunkel, K. E., LeGrande, A. N., & Wehner, M. F. (2017). Temperature changes in the United States. *Climate science special report: Fourth national climate assessment, 1*(GSFC-E-DAA-TN49028).

- 1  
2  
3 Williams, S., Nitschke, M., Sullivan, T., Tucker, G. R., Weinstein, P., Pisaniello, D. L., ... & Bi, P.  
4 (2012). Heat and health in Adelaide, South Australia: assessment of heat thresholds and  
5 temperature relationships. *Science of the Total Environment*, 414, 126-133.  
6  
7  
8 Wolf, T., & McGregor, G. (2013). The development of a heat wave vulnerability index for London,  
9 United Kingdom. *Weather and Climate Extremes*, 1, 59-68.  
10  
11 Zampieri, M., Ceglar, A., Dentener, F., & Toreti, A. (2017). Wheat yield loss attributable to heat  
12 waves, drought and water excess at the global, national and subnational scales. *Environmental*  
13 *Research Letters*, 12(6), 064008.  
14  
15  
16 Zhang, Y., Nitschke, M., Krackowizer, A., Dear, K., Pisaniello, D., Weinstein, P., ... & Bi, P. (2017).  
17 Risk factors for deaths during the 2009 heat wave in Adelaide, Australia: a matched case-  
18 control study. *International journal of biometeorology*, 61(1), 35-47.  
19  
20  
21  
22  
23  
24  
25  
26  
27  
28  
29  
30  
31  
32  
33  
34  
35  
36  
37  
38  
39  
40  
41  
42  
43  
44  
45  
46  
47  
48  
49  
50  
51  
52  
53  
54  
55  
56  
57  
58  
59  
60